# NATIONAL ADVISORY COMMITTEE FOR AERONAUTICS

**TECHNICAL NOTE 4116**

## WIND-TUNNEL INVESTIGATION AT LOW SPEEDS TO DETERMINE FLOW-FIELD CHARACTERISTICS AND GROUND INFLUENCE ON A MODEL WITH JET-AUGMENTED FLAPS

By Raymond D. Vogler and Thomas R. Turner

Langley Aeronautical Laboratory
Langley Field, Va.


Washington
September 1957

NATIONAL ADVISORY COMMITTEE FOR AERONAUTICS

TECHNICAL NOTE 4116

# WIND-TUNNEL INVESTIGATION AT LOW SPEEDS TO DETERMINE FLOW-FIELD CHARACTERISTICS AND GROUND INFLUENCE ON A MODEL WITH JET-AUGMENTED FLAPS

By Raymond D. Vogler and Thomas R. Turner

## SUMMARY

A wind-tunnel investigation has been made at low speeds to determine the flow-field characteristics and ground influence on an airplane model having an untapered, unswept wing with an aspect ratio of 8.3 equipped with jet-augmented flaps. Jet-augmented-flap deflections of 55° and 85° were investigated with the jet-blowing energies covering a range representative of that of the output of current jet airplanes. The high lift coefficients associated with the jet-augmented flaps were greatly reduced when the wing was in the proximity of the ground. The adverse effects of the ground increased rapidly as the wing approached the ground, as the jet-deflection angle increased, or as the momentum coefficient increased. Associated with these reductions in lift coefficient were reductions in both drag coefficient and nose-down pitching-moment coefficient. No ground effect was noted on the model with either a jet-augmented-flap deflection of 55° when the model was mounted higher than 3 chords above the ground or with a jet-augmented-flap deflection of 85° when the model was mounted more than 5 chords above the ground.

High angles of downwash were measured for downstream locations considered of interest for conventional tail locations. The jet-augmented full-span flap produced wing-tip vortices that increased in strength as the jet momentum coefficient increased and resulted in angles of upflow as large as 20° at a location 3 chords behind the wing-tip region.

## INTRODUCTION

As the current design trends continue toward higher cruising speeds and increased wing loading, solutions to the problems of take-off and landing become more difficult. The necessary length of runways and the take-off and landing speeds may be reduced if the lifting power of the wing can be sufficiently increased at low speeds. Some recent investigations (refs. 1 to 4) have shown that remarkably high lift coefficients

can be obtained by exhausting an amount of air corresponding to the full output of current jet engines at or near the trailing edge of the wing. If the jet is directed downward without the use of a physical flap, the arrangement is usually referred to as a jet flap; and if the jet flows over a flap and downward, it is generally called a jet-augmented flap. Results indicate that large lift augmentation is obtained by the increased circulation about the wing in addition to the usual flap and jet-reaction effects. The large lift coefficients obtained on wings with these flaps are usually accompanied by large nose-down pitching-moment coefficients (refs. 1 and 2).

A reasonable assumption is that the exhausting jet can influence the air flow about the wing and at relatively large distances from the wing. The present investigation was made on a model equipped with a jet-augmented flap to study the flow-field characteristics about the wing and in the region of a conventional tail location. A second purpose of the investigation was to determine ground effects on the aerodynamic characteristics of the wing, especially the effect on lift coefficient. The measured data were supplemented by some qualitative photographic tuft studies.

## COEFFICIENTS AND SYMBOLS

The force data are presented with respect to the wind axes with the origin at the wing-root quarter-chord. Signs and symbols used in the presentation of the flow-field data are illustrated in figure 1.

$C_L$ lift coefficient, $\frac{\text{Model lift}}{qS}$

$C_D$ drag coefficient, $\frac{\text{Model drag}}{qS}$

$C_m$ pitching-moment coefficient about wing quarter-chord, $\frac{\text{Model pitching moment}}{qSc}$

$C_\mu$ jet momentum coefficient, $\frac{w_j V_j}{gqS}$

$q$ tunnel dynamic pressure, $\frac{\rho V^2}{2}$, lb/sq ft

$q_l$ local dynamic pressure, $\frac{\rho V_l^2}{2}$, lb/sq ft

$S$ semispan-wing area, 1.50 sq ft

$c$ wing chord, 0.60 ft

$g$ acceleration due to gravity, 32.2 ft/sec$^2$

$\rho$ mass density of air, slugs/cu ft

$V$ free-stream velocity, ft/sec

$V_l$ jet-influenced local velocity, ft/sec

$w_j$ weight rate of air flow through jet slot, lb/sec

$V_j$ jet-exit velocity, isentropic expansion assumed to free-stream static pressure, $\sqrt{\frac{2\gamma}{\gamma - 1} RTg\left[1 - \left(\frac{p}{p_p}\right)^{\frac{\gamma-1}{\gamma}}\right]}$, ft/sec

$\gamma$ ratio of specific heats for air, 1.4

$R$ universal gas constant, $\frac{\text{ft-lb}}{\text{lb}}\Big/{}^{\circ}\text{R}$

$T$ plenum-chamber stagnation temperature, $^{\circ}$R

$p$ free-stream static pressure, lb/sq ft

$p_p$ total pressure in plenum chamber, lb/sq ft

$i_t$ angle of incidence of horizontal tail, measured with respect to wing chord plane, positive when nose deflected upward, deg

$\alpha$ angle of attack of wing chord plane, deg

$\delta$ jet-deflection angle, measured with respect to wing chord plane extended, positive when deflected downward, deg

$\epsilon$ angle of flow, measured with respect to XY-plane, positive downward, deg

$l_X$ longitudinal distance from trailing-edge position of wing at $\alpha = 0^{\circ}$, positive forward of trailing edge, chords

$l_Y$ spanwise distance from XZ-plane, percent of semispan wing

$l_Z$ vertical distance from XY-plane, positive above wing, chords

## APPARATUS AND MODEL

The geometric characteristics of the wing-fuselage model are shown in figure 2. The semispan fuselage was rectangular in cross section except at the nose and in the tail region. The unswept, untapered wing had an aspect ratio of approximately 8.3. The jet-augmented full-span flap was incorporated into the 7.25-inch-chord wing by removing the rear portion of a 10-inch-chord NACA 0012 airfoil section and by installing a 0.75-inch-diameter tube and a plenum chamber. A straight-line fairing from the outer surface of the tube to the lower surface of the wing simulated a very short chord flap. The flap was not free to rotate on the model but would need to rotate for practical application. The chord of the flap was too short to have any particular jet-off aerodynamic significance; and flap deflections of 60° and 90°, measured as shown in figure 2, were simulated in this investigation. Compressed air flowed from the tube into the plenum chamber through 1/16-inch-diameter holes spaced 1/2 inch apart spanwise along the tube. The air flowed from the plenum chamber through a narrow slot in the upper wing surface near the trailing edge, followed the upper surface of the flap, and left the wing at experimentally determined jet-deflection angles of approximately 55° and 85° measured downward from the wing chord plane extended. The method of directing the air into the wing and measuring the weight rate of air flow is described in reference 2.

A ground board spanned the tunnel from wall to wall and extended from approximately 5 feet ahead of the wing to 7 feet behind the wing.

The unswept, untapered horizontal tail had an NACA 0012 airfoil section. The tail and the fuselage were removed for all tests except the force tests involving the horizontal tail.

The instrument used for measuring flow angles and dynamic pressures was mounted on the tunnel survey carriage and is shown in figure 3. The pressure orifices were located about midway between the ends of a 3/16-inch-diameter tube that was normal to the tunnel free stream and parallel to the wing chord plane. There were four orifices around the circumference of the tube as shown. The two that were spaced 35° to either side of the upstream orifice were connected to a pressure cell controlling an electric motor which rotated the tube until the orifice pressures were equalized. In theory, this rotation alined the upstream orifice with the airstream, and the pressure differential between the upstream and downstream orifices (180° apart) was calibrated to be a measure of the dynamic pressure. A factor detrimental to proper tube alinement would be any local velocity gradient across the tube thickness, inasmuch as this gradient could cause the tube to seek an alinement angle in error with the true flow angle; however, it is believed that the instrument was satisfactory for the investigation reported herein. Calibration of the instrument in steady flow indicated that it functioned

well; however, no calibration has been made in unsteady flow. In use, the tube is stationed at the desired survey point and the location, dynamic pressure, and flow angle are indicated on a recording potentiometer. A tuft grid, which indicated flow direction in a plane perpendicular to the tunnel free stream, was made by fastening 2.5-inch-long wool tufts at the intersections of horizontal and vertical fine wires placed 1 inch apart and which were tightly stretched between the sides of a sturdy frame.

A wing having an 18-inch span, a 15-inch chord, and an NACA 0012 airfoil section and equipped with a 12.5-percent-chord jet-augmented flap was used to obtain photographic tuft studies of the flow field about a wing in two-dimensional flow with and without the presence of a ground board. The two-dimensional setup was obtained by mounting the wing between a glass window in the tunnel side wall and a plywood tunnel divider mounted vertically on which tufts were attached. The 12.5-percent-chord flap was deflected approximately 55° and the measured jet deflection was about 50°.

## TEST CONDITIONS AND CORRECTIONS

The semispan models (wing alone and wing plus fuselage and tail) were mounted on the ceiling of the Langley 300-MPH 7- by 10-foot tunnel. Most of the data were obtained at an angle of attack of 0°. The maximum ratios of wing plenum-chamber total pressure to free-stream static pressure were about 4 for the force data and about 5 for the flow surveys. The tunnel dynamic pressures for the tests were 2, 5, and 10 lb/sq ft, and the corresponding Reynolds numbers based on the wing chord were approximately 160,000, 250,000, and 350,000, respectively.

No jet-boundary corrections were applied to the data. Although the lift coefficients were large, the model was relatively small; therefore, the ratio of model area to tunnel area in the correction formula would compensate somewhat for the large lift-coefficient factor. In addition, corrections needed for much of the data would be further reduced by the presence of the ground board.

## RESULTS AND DISCUSSION

### Effects of Ground-Board Distance

The effects of the ground-board distance on the lift, pitching-moment, and drag characteristics of the wing alone with jet-augmented flaps deflected 55° and 85° are shown in figures 4 to 7 with $\alpha = 0°$

and $q$ = 2 and 10 lb/sq ft. The lower tunnel dynamic pressure gives a greater range of momentum coefficients, and the higher tunnel dynamic pressure gives less scatter of data points at low momentum coefficients. A comparison of the data shows that the results are not affected by this change in test dynamic pressure. The effect of angle of attack on the lift and pitching-moment coefficients of the wing with a flap deflection of 55° at a rather small momentum coefficient (0.65) is shown in figure 8 with $q$ = 10 lb/sq ft. Cross plots of the lift data against ground-board distance for a range of momentum coefficients, taken from figures 4 and 6, are presented in figure 9 to show the relative effectiveness of the jet-augmented flap at $\delta$ = 55° and 85° as the wing nears the ground.

For the range of conditions investigated, no significant lift increases were obtained as a result of ground-board proximity, but as the wing with the flap deflected 55° came closer than 3 chords to the ground or as the wing with the flap deflected 85° came closer than 5 chords to the ground, large decreases in lift resulted for various combinations of ground-board distances and momentum coefficients (figs. 4, 6, and 9). The momentum coefficient at which lift losses first occurred was reduced as the ground-board distance was reduced; and for a given ground-board distance, increases in momentum coefficient above this initial value generally increased the magnitude of the lift loss. As shown in figure 9, the lift loss at a given ground-board distance is less for the jet-augmented flap deflected 55° than for the jet-augmented flap deflected 85°. This result is in qualitative agreement with the still lower losses for a deflection of 35° shown in reference 3. At the very low momentum coefficients ($C_\mu < 0.3$), the range that might be of more interest in boundary-layer control, the lift for both flap deflections was generally affected only slightly by the ground board at any distances tested (figs. 4 and 6). At a rather low momentum coefficient (0.65), ground-board distances of 1 chord or more had little effect on the general variation of $C_L$ with $\alpha$ for the jet-augmented flap deflected 55°, except at larger angles of attack at which the jet was effectively brought closer to the ground board and thereby caused some loss in lift (fig. 8). With a ground-board distance of 1/2 chord, large lift losses occurred throughout the angle-of-attack range.

The large nose-down pitching-moment coefficients of the wing alone are reduced by the presence of the ground board (figs. 4 and 6). This reduction would be expected as it parallels the lift reduction caused by the ground board. Some of the pitching-moment data show considerable data-point scatter, however, as a result of the very low tunnel dynamic pressure.

Without the presence of the ground board the wing with the flap deflected 85° (fig. 5) has large positive drag coefficients; whereas the wing with the flap deflected 55° (fig. 7) produces large negative drag coefficients as a result of a larger component of jet reaction being in

the thrust direction. However, for both deflections, the lift loss resulting from the presence of the ground board is accompanied by a reduction in drag coefficient, or, for the flap deflection of 55°, by an increase in thrust.

The tuft studies shown in figure 10 were made by using the wing with a 12.5-percent-chord jet-augmented flap in two-dimensional flow. The tufts and the long streamers attached to the wing indicate the flow field about the wing without a ground board and with a ground board approximately 1 chord below the wing. As reported in previous investigations (refs. 1 to 4), the increased lift of a wing with jet-augmented flaps results from increased circulation and jet reaction. Evidence of increased circulation as the momentum coefficient is increased is shown by the larger angles of upflow in front of the wing and the larger angles of downflow behind the wing. The effect of the ground board is small at a momentum coefficient of 1, but at a momentum coefficient of 5 the effect of the ground board as shown by the tuft pattern is very noticeable. Some of the jet stream is deflected upstream by the ground board and thus results in what appears to be a large captive vortex between the wing and the ground board. In addition, a large area behind the wing and behind the jet sheet is filled with turbulent flow. These flow changes should account for much of the lift loss shown in figures 4 and 6.

## Flow-Field Characteristics

Studies, confined primarily to the region of conventional tail locations, were made by means of force tests and a flow-angle indicator of the flow-field characteristics about the model equipped with a jet-augmented flap. The force tests were made on a semispan model that included a typical tail, and the surveys made with the flow-angle indicator were made on the wing alone. The pitching-moment characteristics of the semispan model with and without blowing are shown in figures 11 and 12, respectively. Without the jet blowing (fig. 12(a)), the model is either neutrally stable or stable, and only small tail deflections would be necessary to trim the model for lift coefficients up to 1.2 ($\alpha \approx 10^\circ$). With the jet-augmented flap deflected 55° and operating at near-maximum test pressure (fig. 12(b)), the increased lift coefficients are accompanied by large nose-down pitching-moment coefficients. The variation of lift and pitching-moment coefficients with momentum coefficient (fig. 11) is typical of results reported previously (refs. 1 and 2) where the jet-blowing energy involved is far in excess of that needed for flow attachment for boundary-layer control. If the effect of tail drag on the pitching moment is disregarded, the results given in figure 12(b) indicate that the horizontal tail is probably stalled at an angle of incidence of 0°. The pitching-moment data of figure 11 show that the direction of the lift force on the tail reverses at angles of incidence

of the tail of 15° or 20° depending upon the momentum coefficient. This fact would indicate an integrated angle of downflow of roughly 15° or 20° in the region of the tail. This tail, with an area approximately one-fourth of that of the wing, produces only about one-fourth the pitching moment required to trim the model at a momentum coefficient of 2.70 corresponding to lift coefficients of 7.0. This fact indicates the need for a more powerful tail, a change in center-of-gravity location, or another type of control. The results of using some of these methods to trim a swept-wing model with a different type of jet-augmented flap are given in reference 5. The most favorable factors for producing trim conditions were not sought in the present investigation. For example, as shown in reference 2, the nose-down pitching moments of a jet-augmented flap having a longer chord are smaller than those of the present investigation. Installing a jet-augmented tail surface would probably increase the tail lift coefficient the necessary four times, but since the downward force on the tail would be considerable, changing to a canard surface would probably improve the overall lifting ability of the model (ref. 6).

The flow angles and local dynamic pressures measured at various positions in the flow field of the wing alone are given in figures 13 to 17 for the wing with the jet-augmented flap deflected 55° and in figures 18 and 19 for the wing with the jet-augmented flap deflected 85°. Many curves show pronounced local flow-angle irregularities occurring at data points that represent locations in and near the high-velocity jet stream. These flow-angle irregularities could possibly be caused by local velocity-gradient effects on the flow-measuring instrument, as previously discussed; however, a turbulent mixing region would be expected on either side of the core of the jet and local flow-angle irregularities might predominate in this region. Inasmuch as the overall magnitudes were considered to be of the most significance, no attempt was made to study these local-flow effects.

For the downstream locations surveyed (fig. 13), the angle of downflow, or angle of downwash, and the local dynamic pressure increase as the jet momentum coefficient increases. The increase in local dynamic pressure is confined primarily to the region of the jet, whereas the angle of downwash is increased over a large vertical distance. As might be expected, the jet center as defined by the maximum local dynamic pressure is deflected less by the free stream as the jet momentum coefficient increases. The angle of downwash at the location occupied by the horizontal tail in the force tests is estimated to be about 17° at a momentum coefficient between 1.67 and 3.20. This angle is in agreement with the angle of downwash indicated by the force tests and discussed previously. Figures 14 and 15 show the large variation of flow angle with spanwise location, measured from 1 to 3 chords behind the trailing edge, at momentum coefficients of 1.67 and 6.46, respectively. The indicated variation due to spanwise location is not very large from the root chord

to the 75-percent-semispan station; but near the tip, large (20° to 30°) angles of upflow, or upwash, occur. This large reversal of flow direction most likely results from strong vortices from the wing tip. In general, the results of these tests with the jet-augmented flap deflected 55° and the wing at an angle of attack of 0° indicate that the average angle of downwash measured on the extended chord plane, between the vertical plane of symmetry and the 50-percent-semispan station, and at a location 3 chords behind the wing trailing edge, varies from 14° to 40° for momentum coefficients from 0.61 to 6.46.

In order to help complete the flow-field study about the wing, the chordwise locations indicated in figure 16 were surveyed. The sharp angles of upwash occurring ahead of the wing increase as the momentum coefficient increases. The effects of varying the wing angle of attack on the flow characteristics at two downstream survey locations are shown in figure 17. Most of the changes in flow with changes in angle of attack shown in figure 17 would be expected since the flow angles were measured with respect to the XY-plane of the wind axis and a change in angle of attack was effectively a change in jet-deflection angle with respect to that plane. In general, the downward movement of the jet center with increasing angle of attack is indicated by the relative locations of the data points of maximum local dynamic pressure; however, the jet-center location as indicated for $\alpha = 12^\circ$ in figure 17(a) is not readily explained but may have been influenced by the wing-tip vortex. Figures 18 and 19 show that the results of flow surveys at various spanwise locations behind the jet-augmented flap deflected 85° are similar to the results shown in figure 14 for the jet-augmented flap deflected 55° in that vortices produce large peak angles of upwash and downwash at outboard locations below the chord plane. An increase in momentum coefficient increases the overall angles of downwash as well as the maximum peaks of angles of upwash and downwash.

Photographs are given in figures 20 to 22 of the tuft grid mounted 2.5 chords behind the trailing edge of the wing alone of the model (fig. 2). The camera view is from behind the wing, and the lower surface of the wing is to the left. The tunnel dynamic pressure for all the tuft-grid tests was 2 lb/sq ft. The tuft pattern roughly indicates crossflow by the directions and projected relative lengths of the tufts. Distances between the heavy dots at the grid margin represent approximate chord lengths. Only small or no wing-tip vortices are indicated with no blowing from the jet slot as the wing is rotated through a range of $\alpha$ (fig. 20); but at a constant momentum coefficient of 3.28 (fig. 21), the tuft pattern indicates a large field of strong downflow and a very pronounced wing-tip vortex producing local upflows. The flow characteristics increase in intensity as the momentum coefficient of the jet increases as shown in figure 22.

## CONCLUSIONS

A wind-tunnel investigation was made at low speeds to determine the flow-field characteristics and ground effects on an airplane model having an untapered, unswept wing with an aspect ratio of 8.3 equipped with a jet-augmented flap. Jet-augmented-flap deflections of 55° and 85° were tested, and the jet-blowing energies covered a range representative of that of the output of current jet airplanes. From the data obtained, the following conclusions are made:

1. The high lift coefficients produced by jet-augmented flaps are greatly reduced by bringing the wing closer than 3 chords to the ground for a flap deflection of 55° or 5 chords to the ground for a flap deflection of 85°. The adverse effects of the ground increase rapidly as the wing approaches the ground, as the flap-deflection angle increases, or as the momentum coefficient increases.

2. In the presence of the ground, the drag coefficients are reduced and the pitching-moment coefficients of the wing about the quarter-chord become less negative.

3. Regions of high downwash were measured for downstream locations considered of interest for conventional tail locations. For example, with the jet-augmented flap deflected 55° and the wing at an angle of attack of 0°, angles of downwash measured inboard and 3 chords behind the wing on the wing chord plane extended varied from 14° to 40° for momentum coefficients from 0.61 to 6.46.

4. Jet-augmented full-span flaps produce wing-tip vortices that increase in strength as the jet momentum coefficient increases and result in angles of upflow as large as 20° at a location 3 chords behind the wing-tip region.

Langley Aeronautical Laboratory,
National Advisory Committee for Aeronautics,
Langley Field, Va., July 10, 1957.

## REFERENCES

1. Lowry, John G., and Vogler, Raymond D.: Wind-Tunnel Investigation at Low Speeds To Determine the Effect of Aspect Ratio and End Plates on a Rectangular Wing With Jet Flaps Deflected 85°. NACA TN 3863, 1956.

2. Lockwood, Vernard E., Turner, Thomas R., and Riebe, John M.: Wind-Tunnel Investigation of Jet-Augmented Flaps on a Rectangular Wing to High Momentum Coefficients. NACA TN 3865, 1956.

3. Dimmock, N. A.: An Experimental Introduction to the Jet Flap. National Gas Turbine Establishment Rep. No. R.175, British Ministry of Supply, Apr. 1955.

4. Malavard, L., Poisson-Quinton, Ph., Jousserandot, P. (T. M. Berthoff and D. C. Hazen, trans.): Theoretical and Experimental Investigations of Circulation Control. Rep. No. 358, Princeton Univ., Dept. Aero. Eng., July 1956.

5. Campbell, John P., and Johnson, Joseph L., Jr.: Wind-Tunnel Investigation of an External-Flow Jet-Augmented Slotted Flap Suitable for Application to Airplanes With Pod-Mounted Jet Engines. NACA TN 3898, 1956.

6. Lowry, John G., Riebe, John M., and Campbell, John P.: The Jet-Augmented Flap. Preprint No. 715, S.M.F. Fund Paper, Inst. Aero. Sci., Jan. 1957.

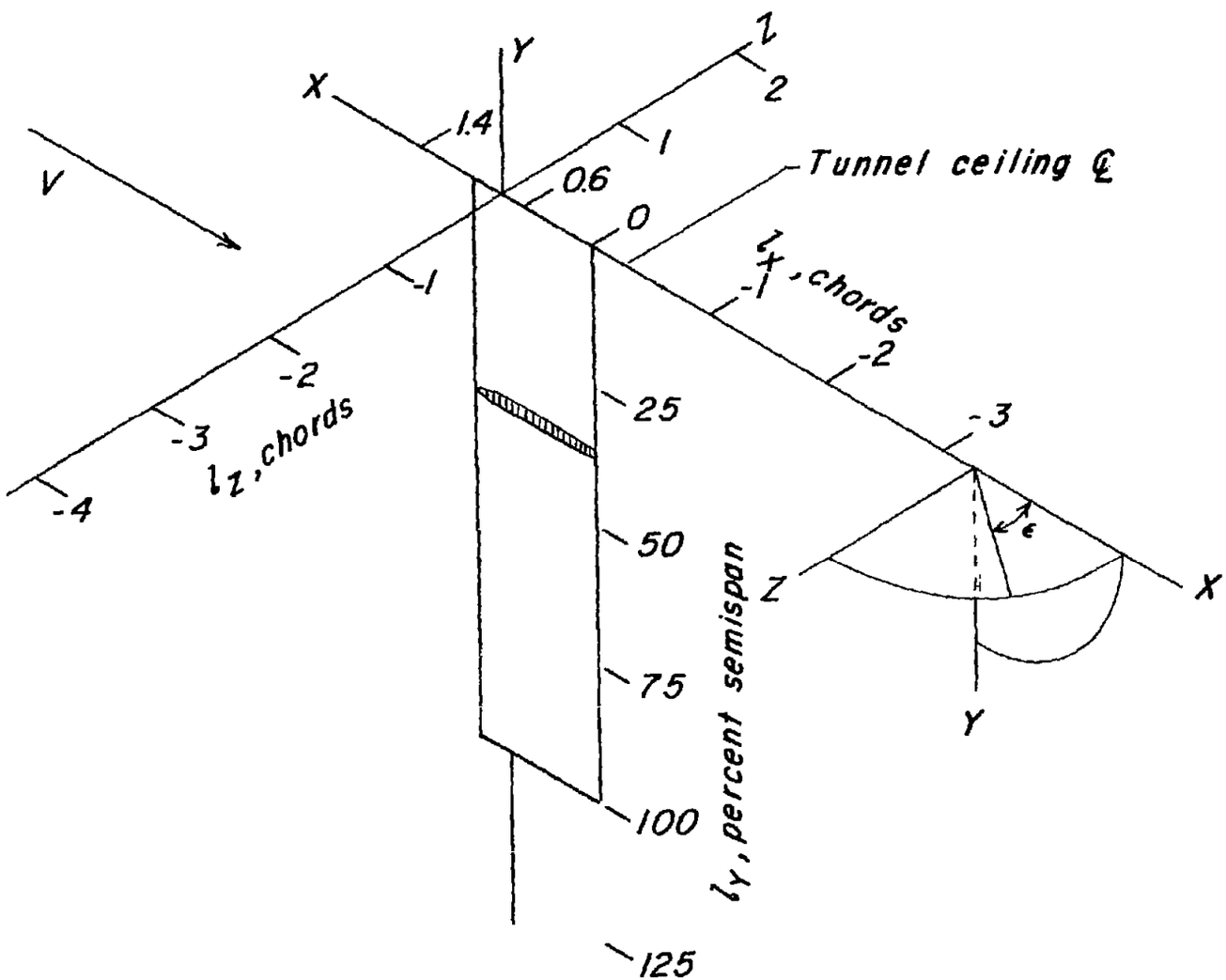


Figure 1.- Wind axes system used in presentation of flow-field data of semispan wing mounted on tunnel ceiling.

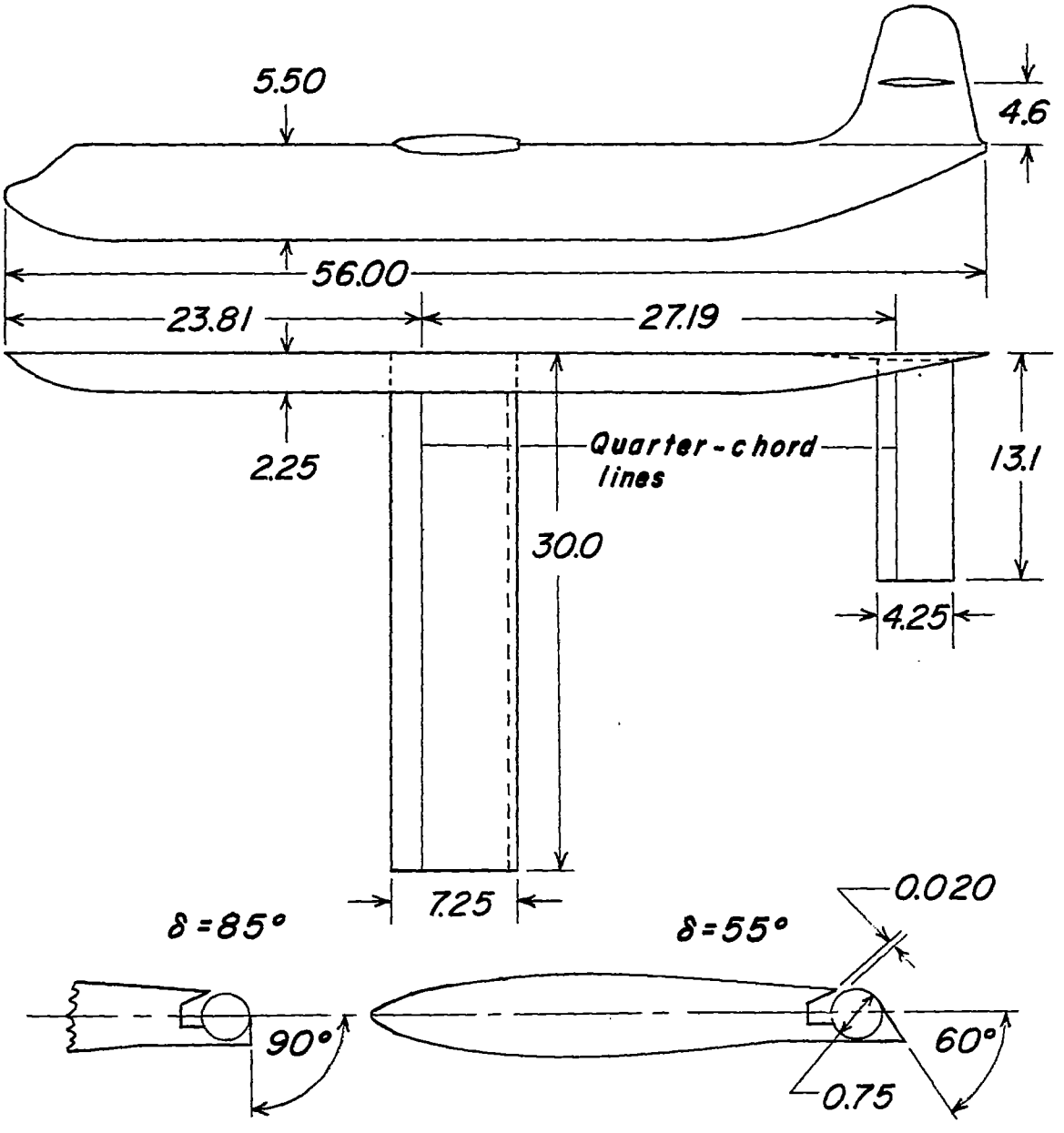


Figure 2.- Details of complete semispan model. All dimensions are in inches.

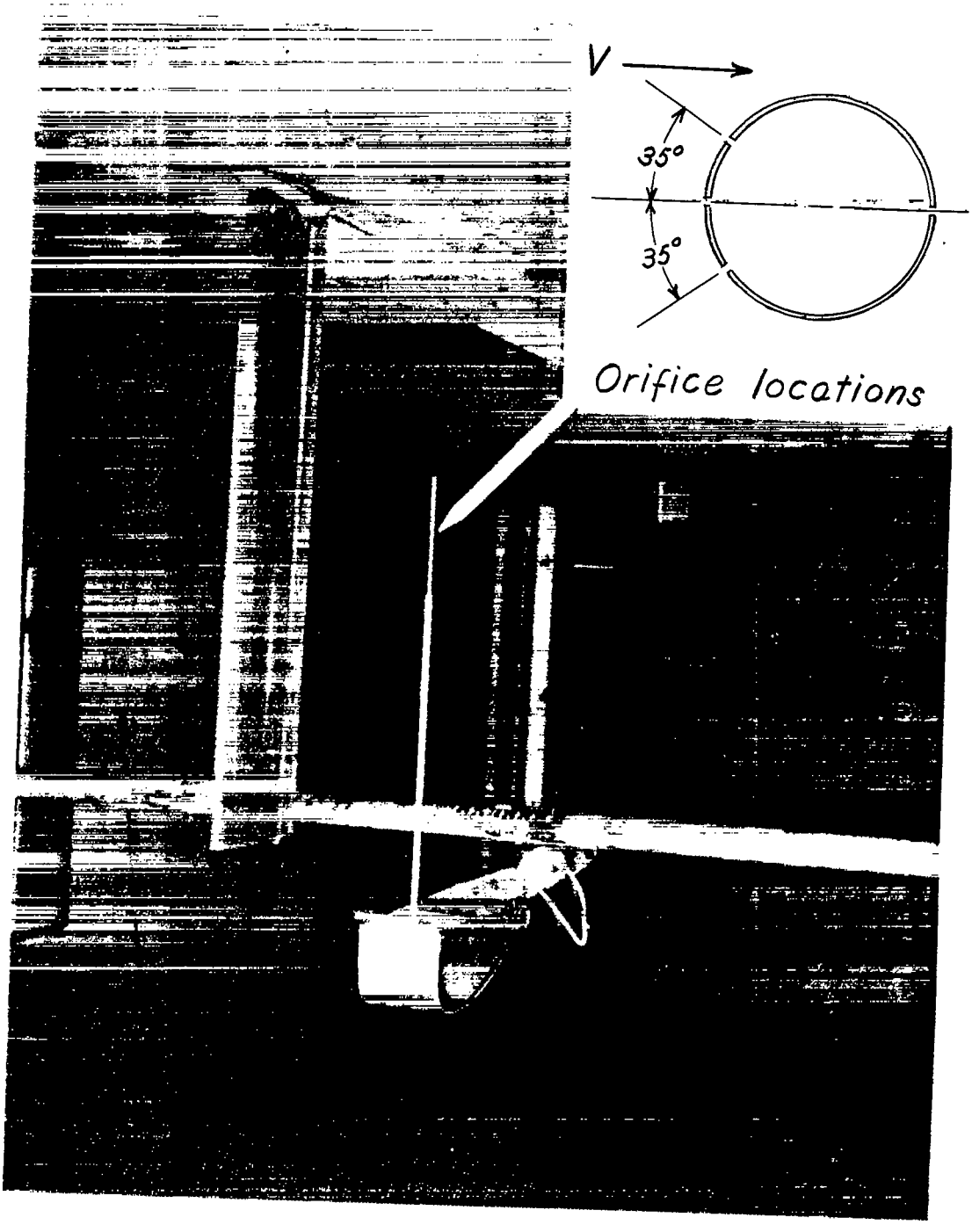


L-94816

Figure 3.- Photograph of wing alone showing flow-angle and dynamic-pressure indicator mounted on tunnel survey carriage.

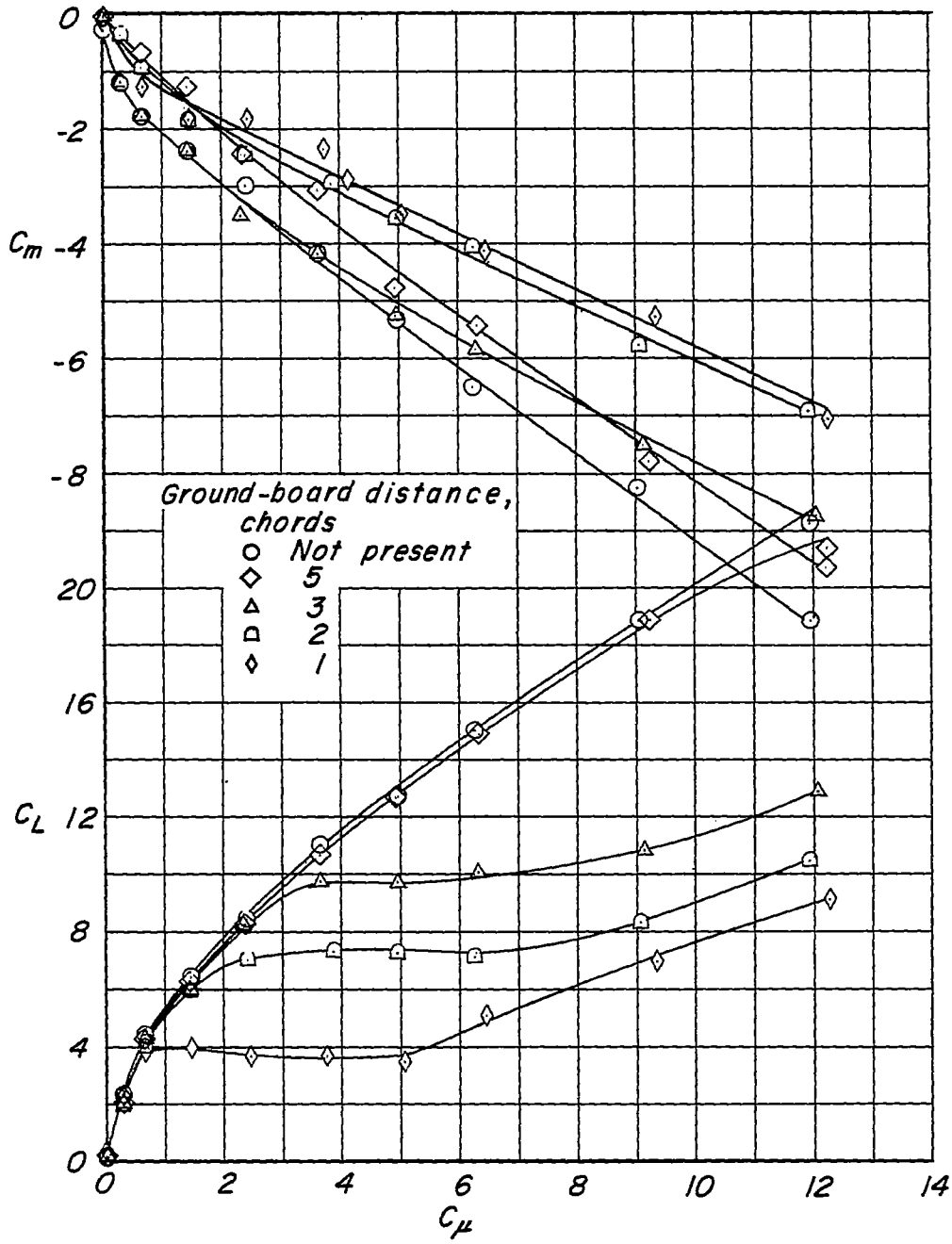


(a) q = 2 lb/sq ft.

Figure 4.- Effect of ground-board distance on lift and pitching-moment coefficients of wing. $\delta = 85^\circ$; $\alpha = 0^\circ$.

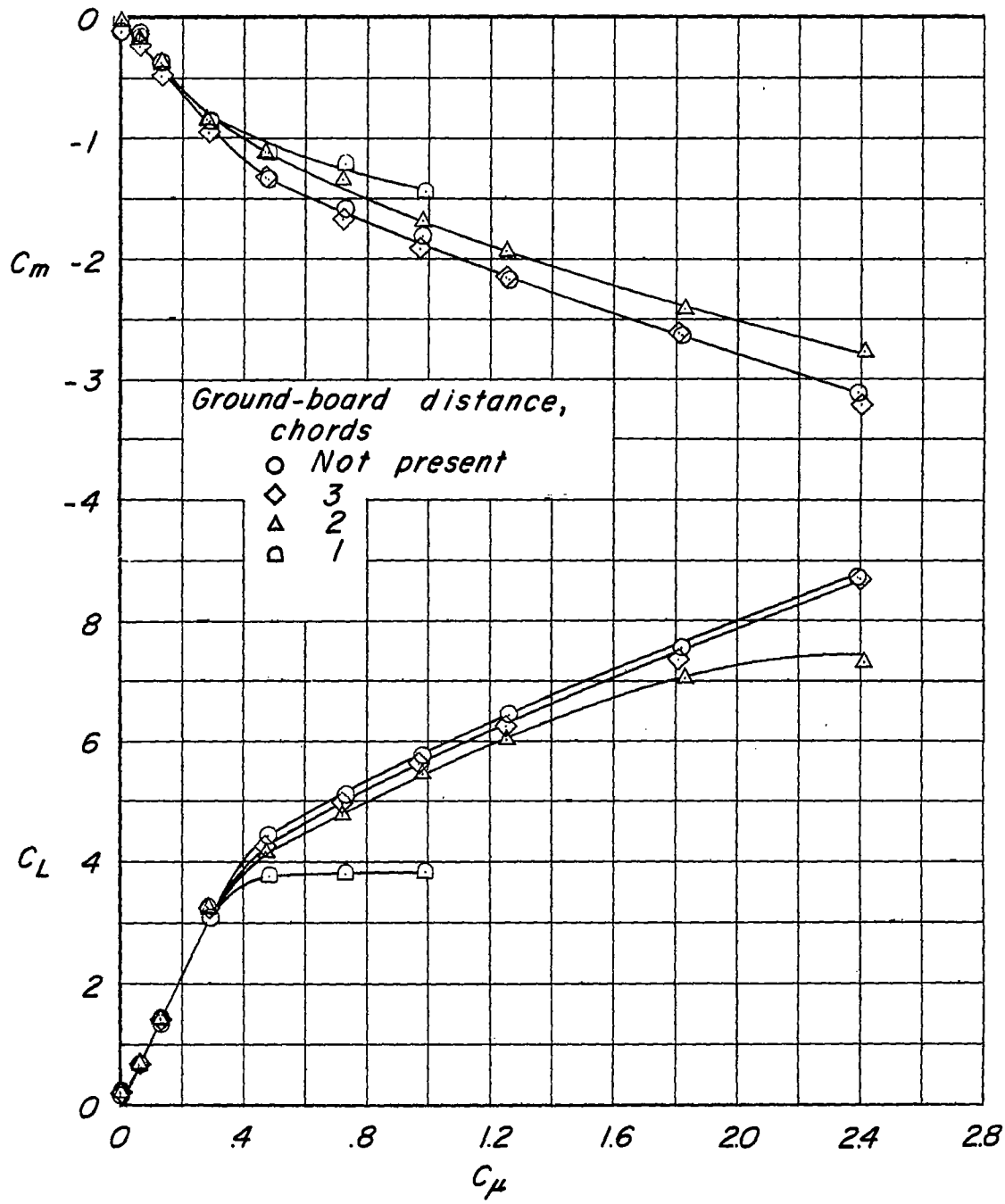


(b) q = 10 lb/sq ft.

Figure 4.- Concluded.

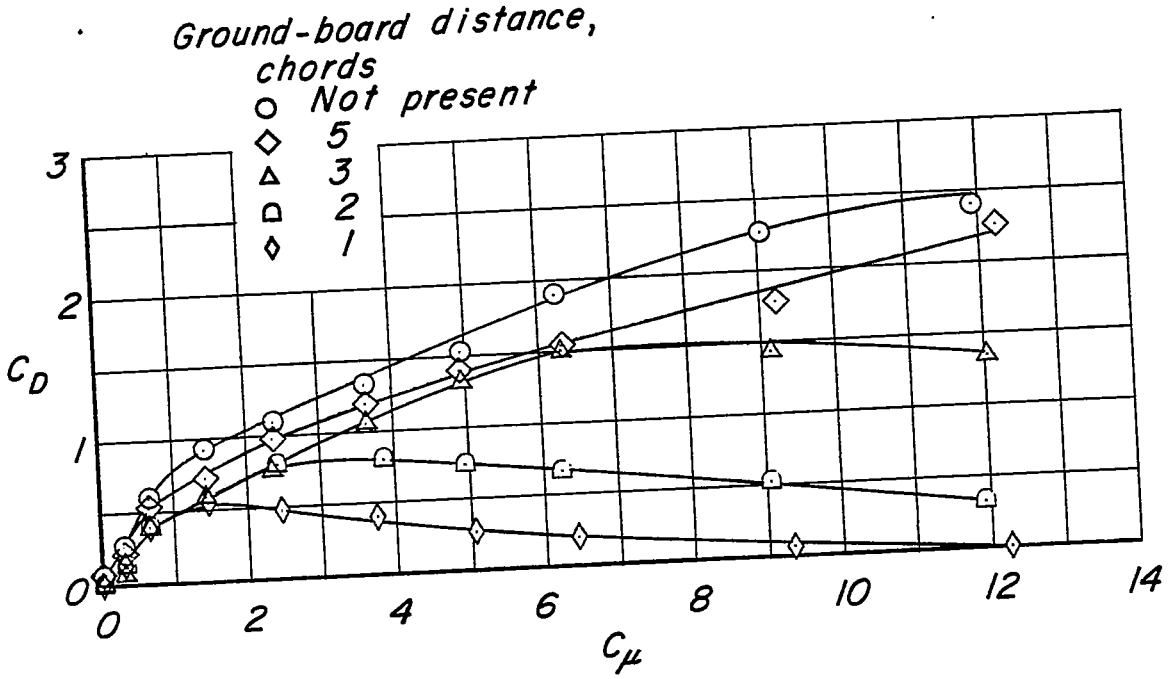


(a) q = 2 lb/sq ft.

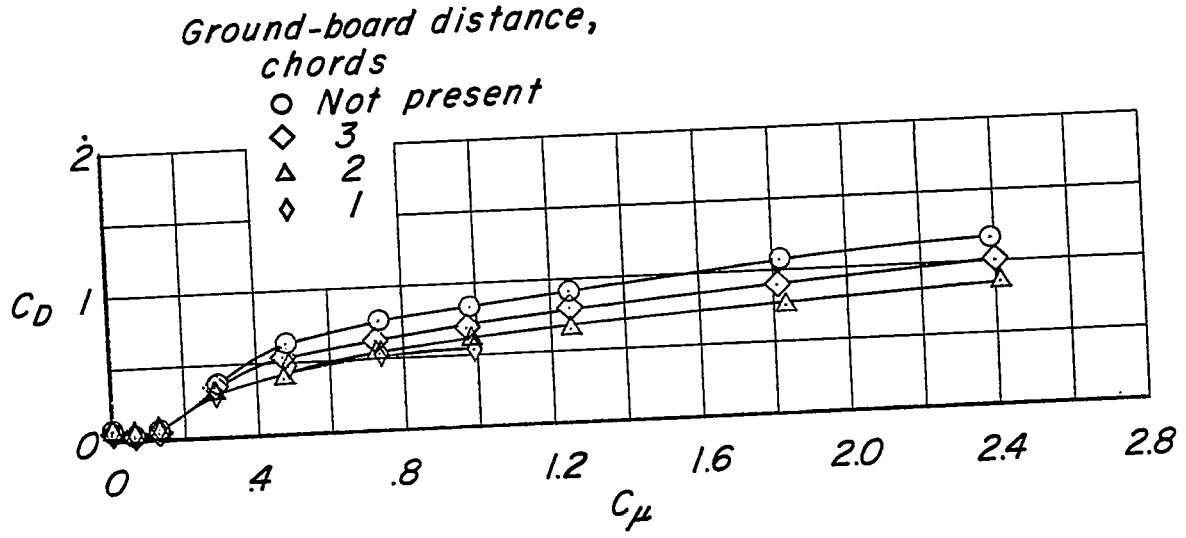


(b) q = 10 lb/sq ft.

Figure 5.- Effect of ground-board distance on drag characteristics of wing. $\delta = 85^\circ$; $\alpha = 0^\circ$.

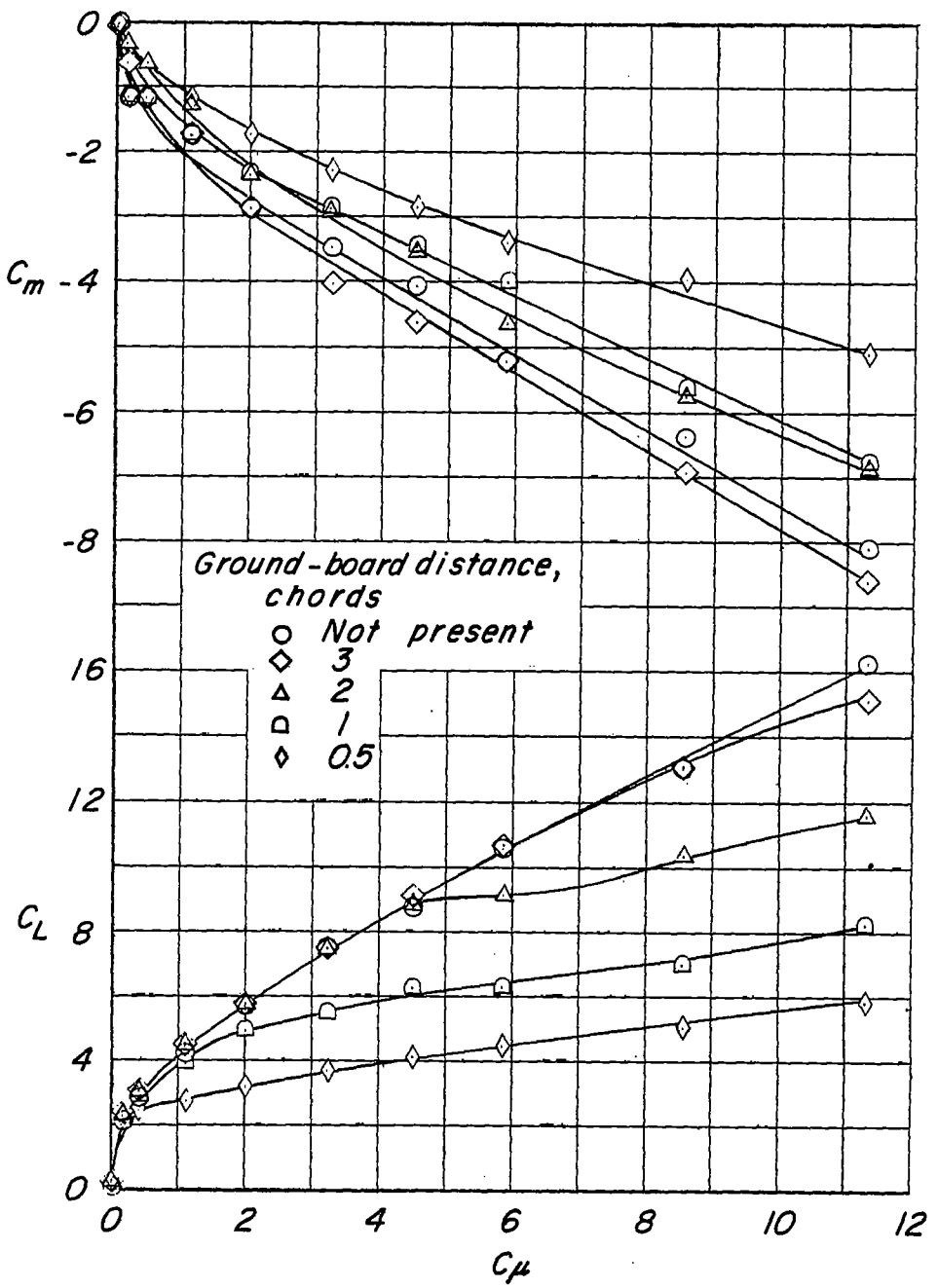


(a) q = 2 lb/sq ft.

Figure 6.- Effect of ground-board distance on lift and pitching-moment coefficients of wing. $\delta = 55^\circ$; $\alpha = 0^\circ$.

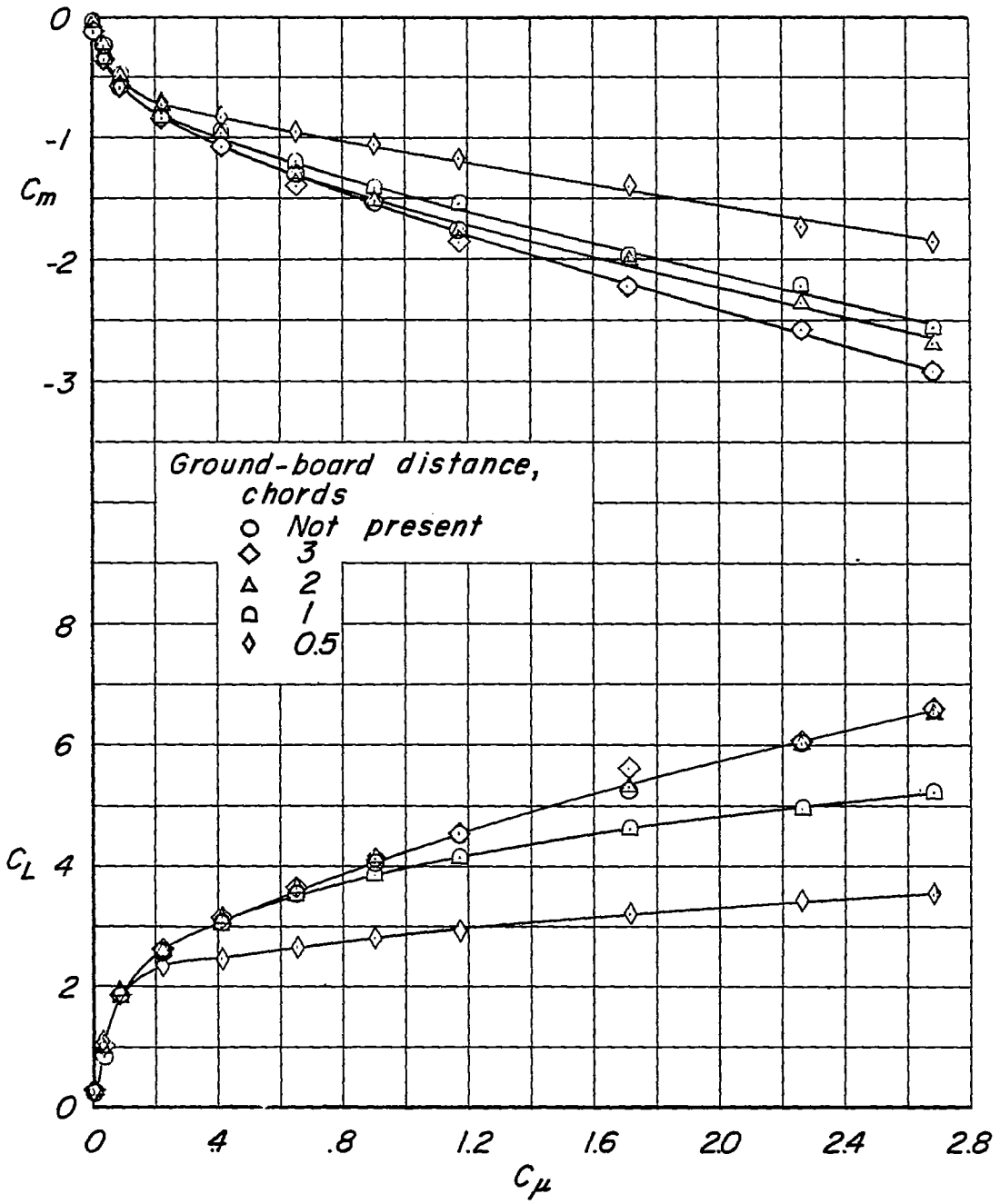


(b) q = 10 lb/sq ft.

Figure 6.- Concluded.

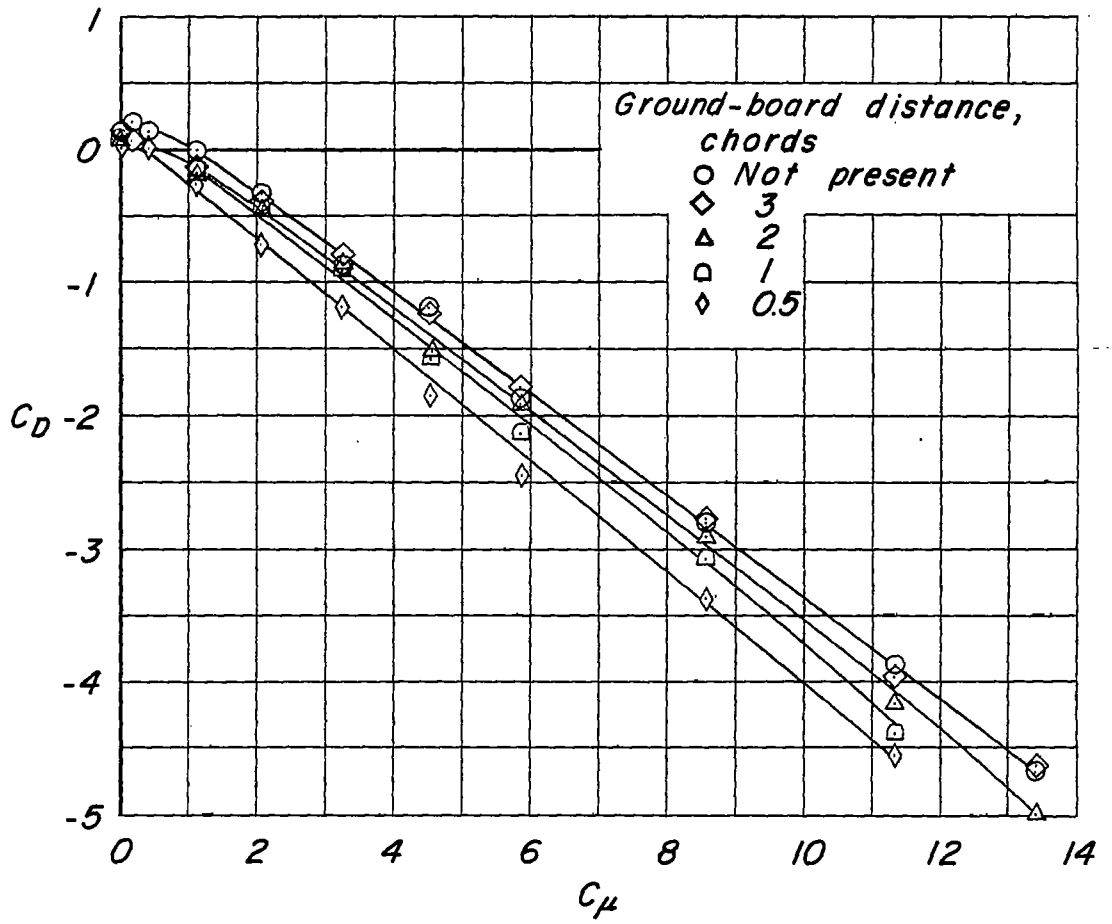


(a) q = 2 lb/sq ft.

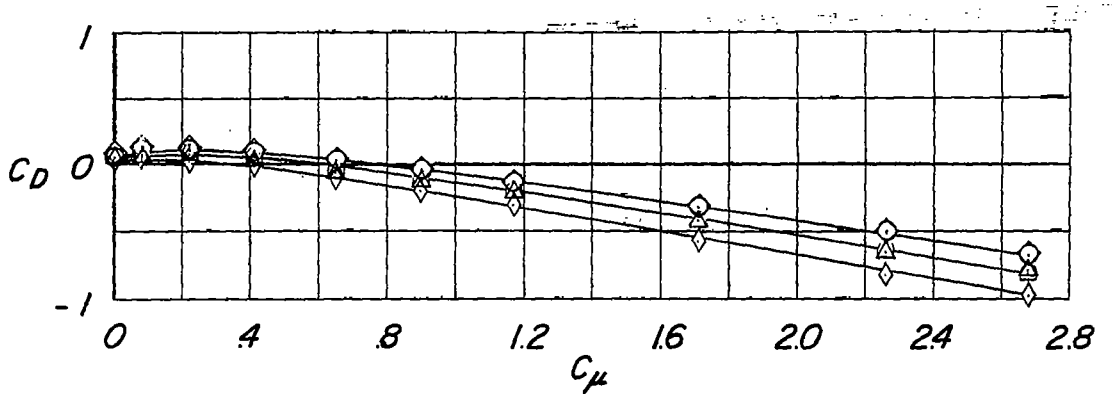


(b) q = 10 lb/sq ft.

Figure 7.- Effect of ground-board distance on drag characteristics of wing. $\delta = 55^\circ$; $\alpha = 0^\circ$.

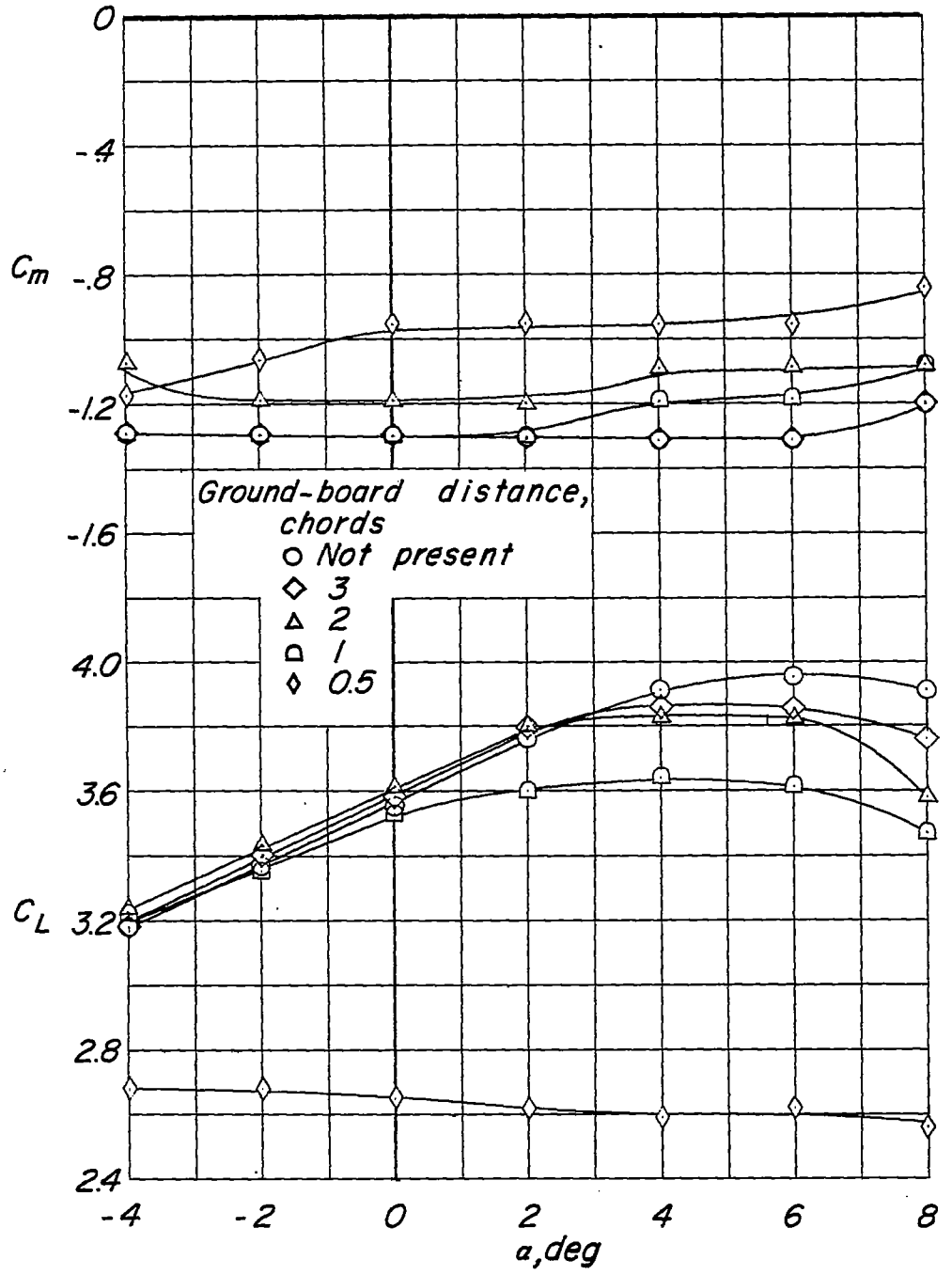


Figure 8.- Effect of ground-board distance on variation of lift and pitching-moment coefficients of wing with angle of attack. $\delta = 55°$; $C_\mu = 0.65$; $q = 10$ lb/sq ft.

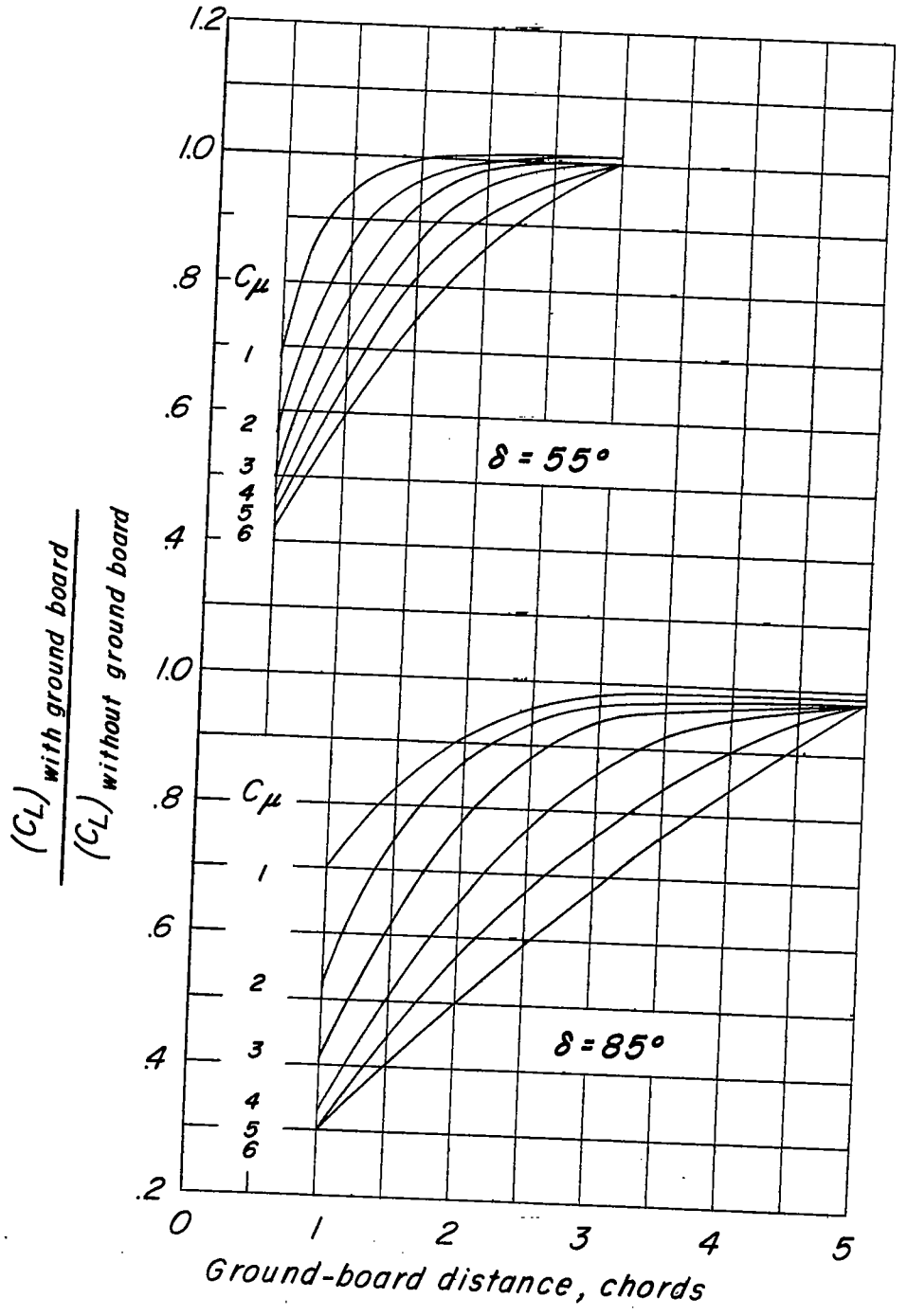


Figure 9.- Ratio of lift coefficient with ground board to lift coefficient without ground board for a range of ground-board distances and momentum coefficients for wing with $\delta = 55°$ and $85°$.

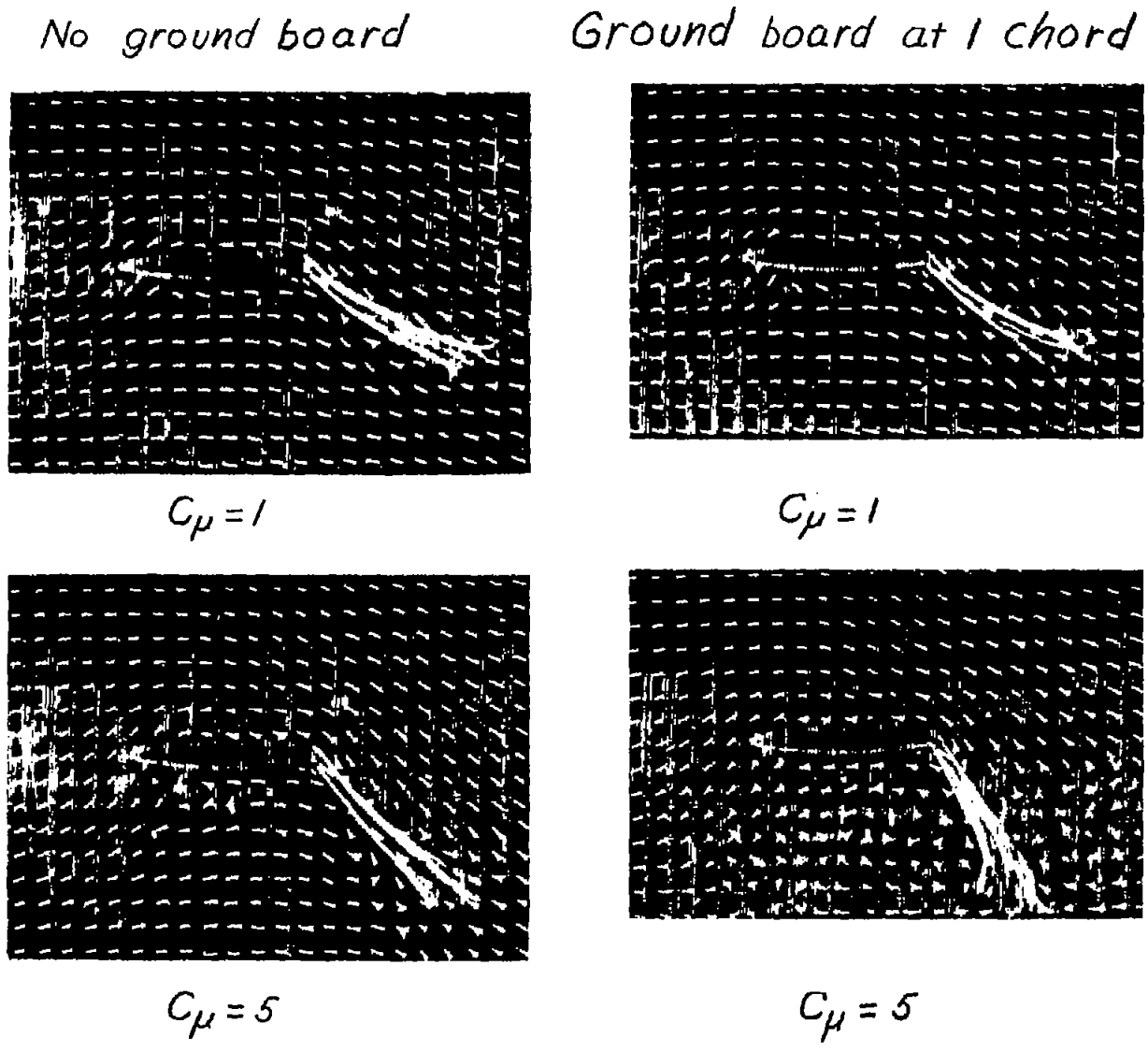


L-57-2717

Figure 10.- Tufts in two-dimensional-flow field of 15-inch-chord wing with 12.5-percent-chord jet-augmented flap without and with a ground board 1 chord below wing. $\alpha = 0^\circ$; $\delta \approx 50^\circ$; $q = 2$ lb/sq ft.

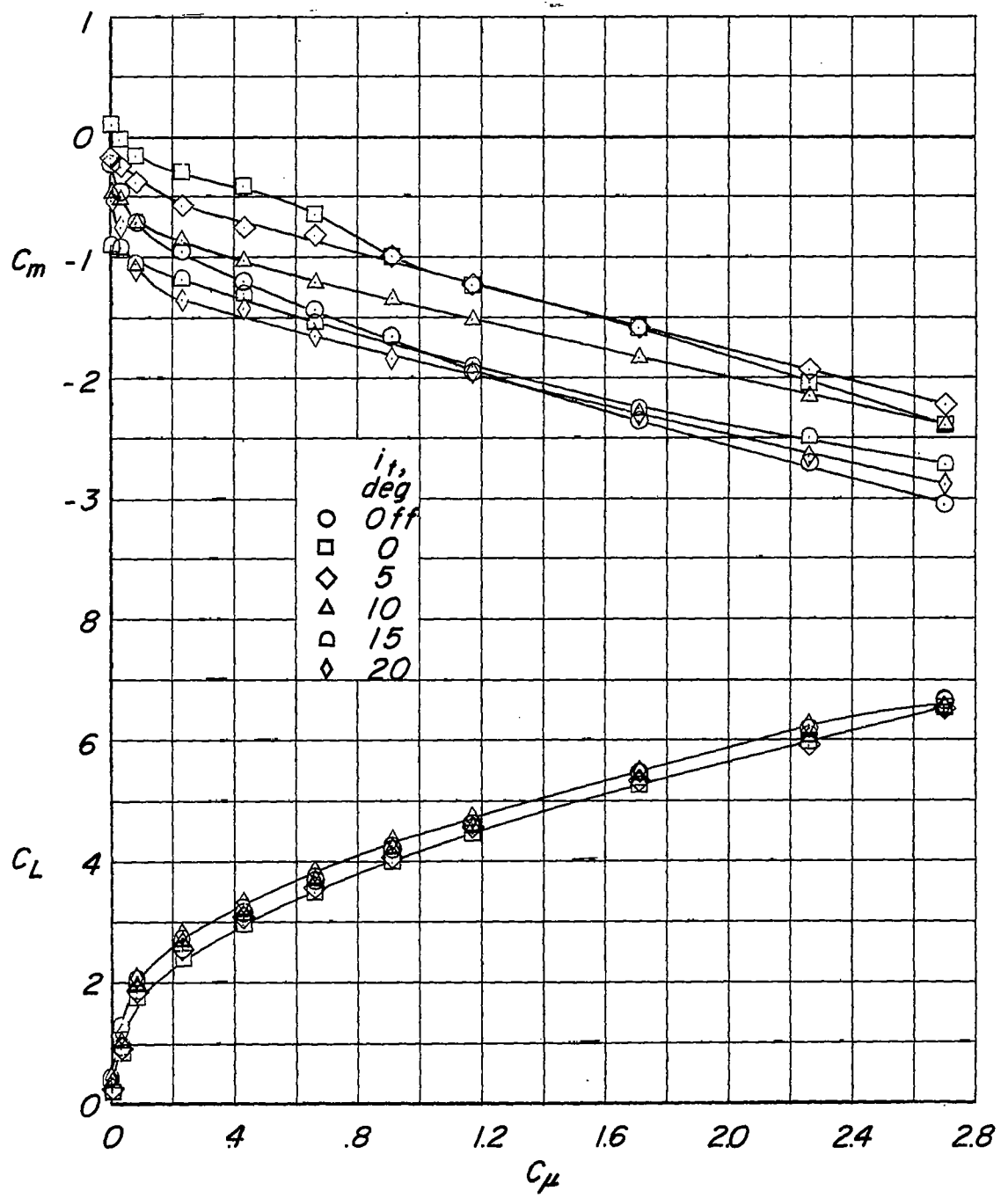


Figure 11.- Variation of lift and pitching-moment coefficients of model with momentum coefficient for various angles of incidence of horizontal tail. $\delta = 55°$; $\alpha = 0°$; $q = 10$ lb/sq ft.

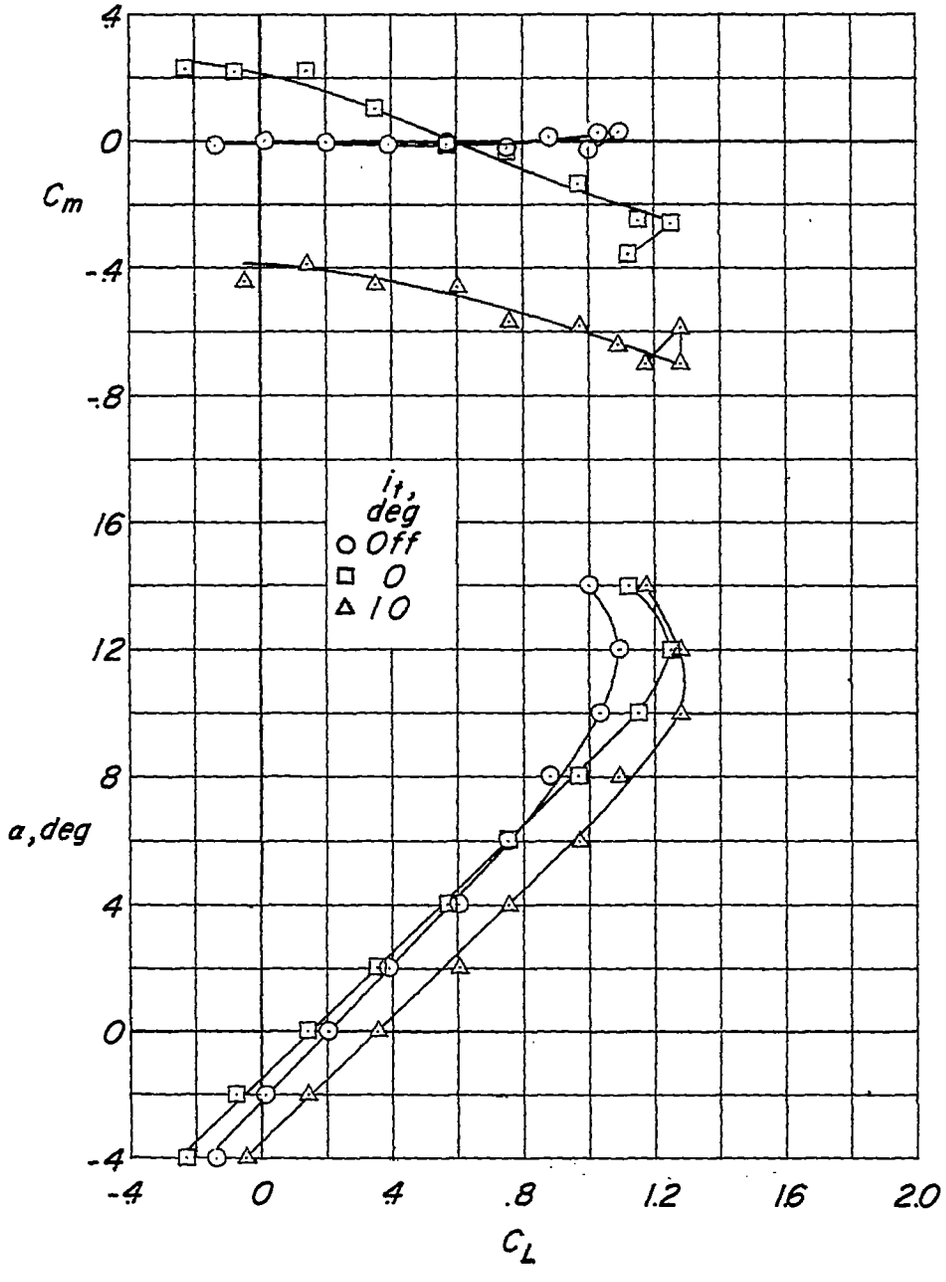


(a) $C_\mu = 0$.

Figure 12.- Effect of various angles of incidence of horizontal tail on model aerodynamic characteristics in pitch. $\delta = 55^\circ$; q = 10 lb/sq ft.

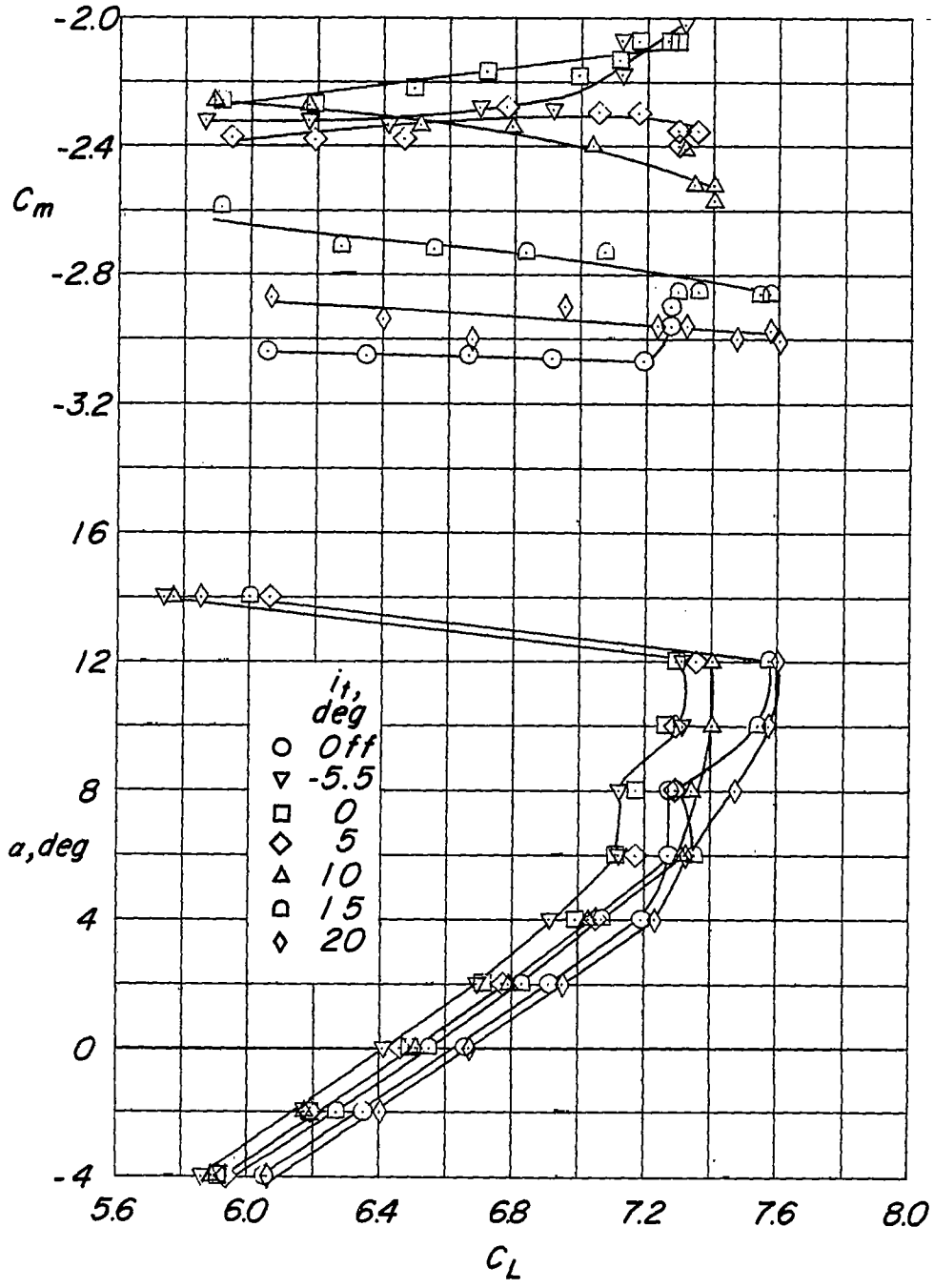


(b) $C_\mu$ = 2.70.

Figure 12.- Concluded.

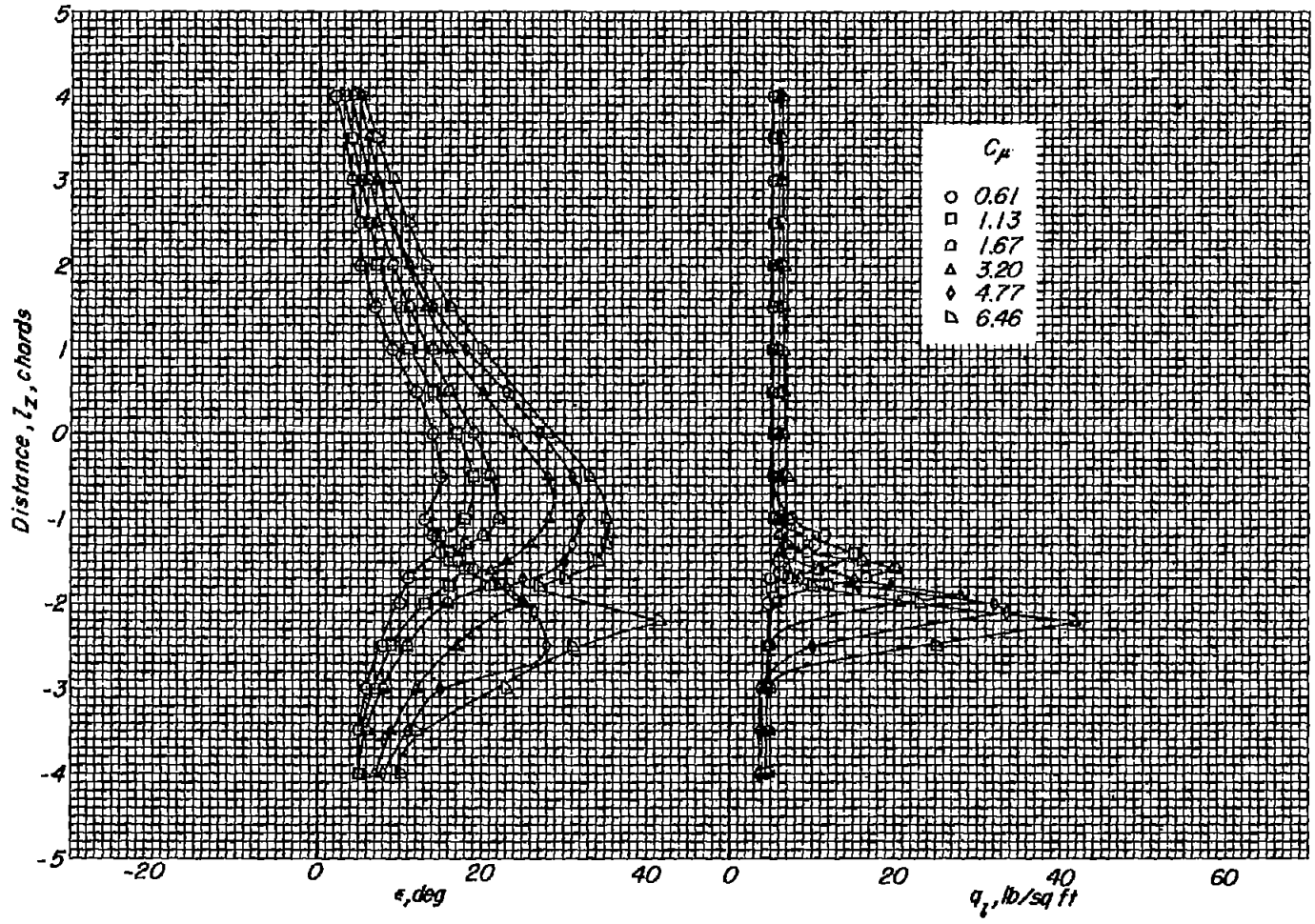


(a) $l_X$ = -3 chords.

Figure 13.- Effect of momentum coefficient on flow angle and local dynamic pressure behind wing. $\delta = 55^\circ$; $l_Y$ = 50-percent-semispan station; $\alpha = 0^\circ$; q = 5 lb/sq ft.

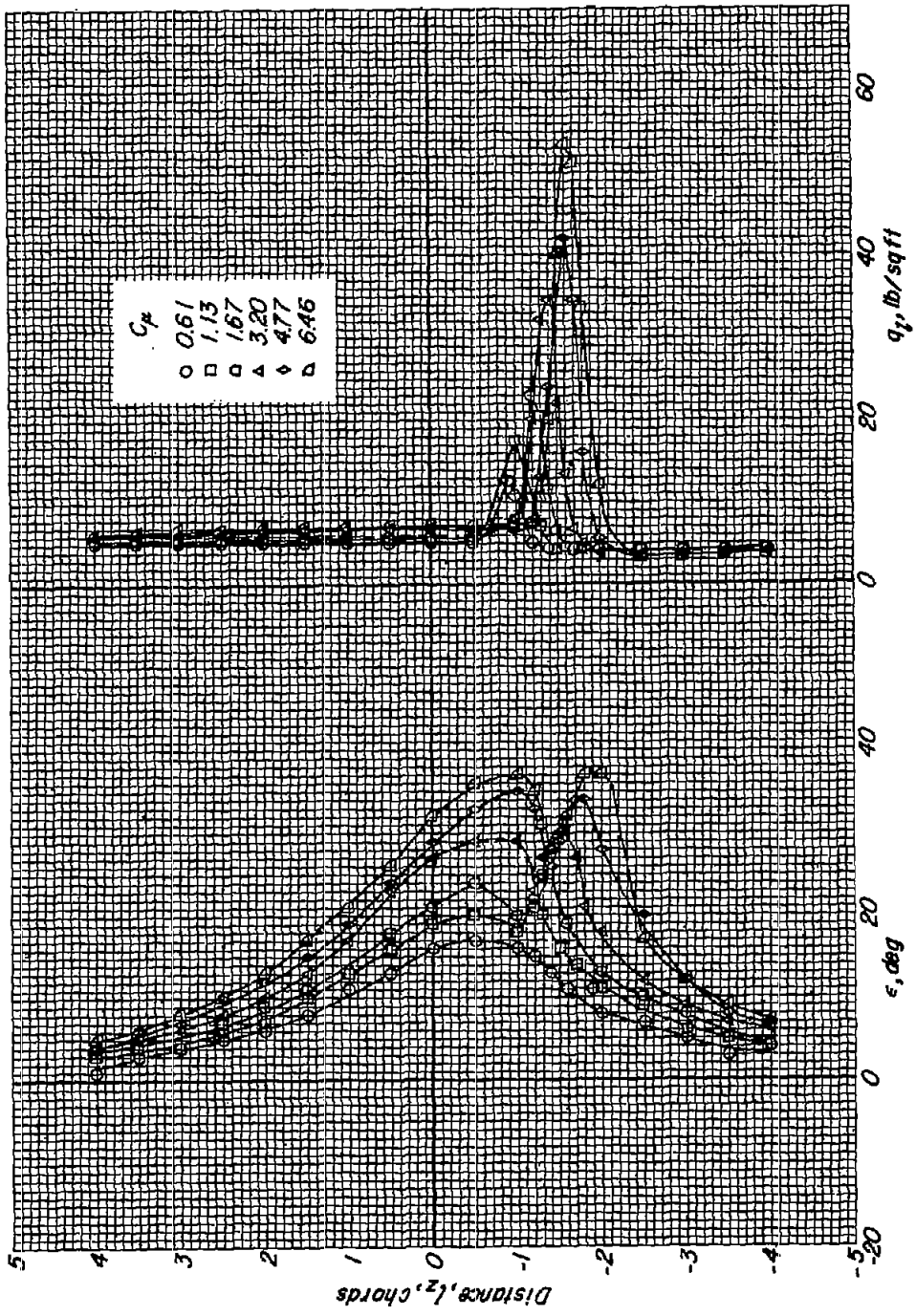


(b) $l_X$ = -2 chords.

Figure 13.- Continued.

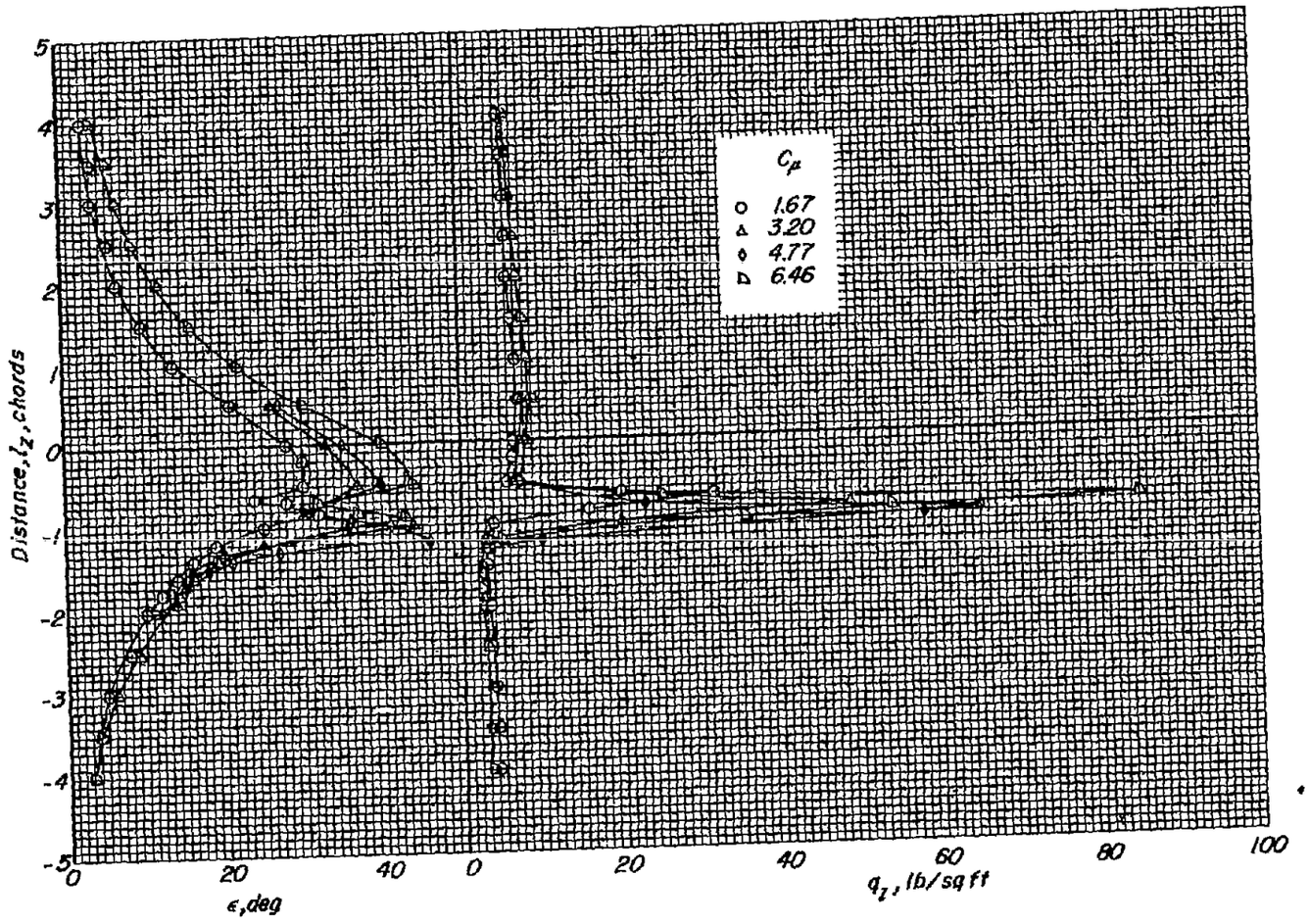


(c) $l_X$ = -1 chord.

Figure 13.- Concluded.

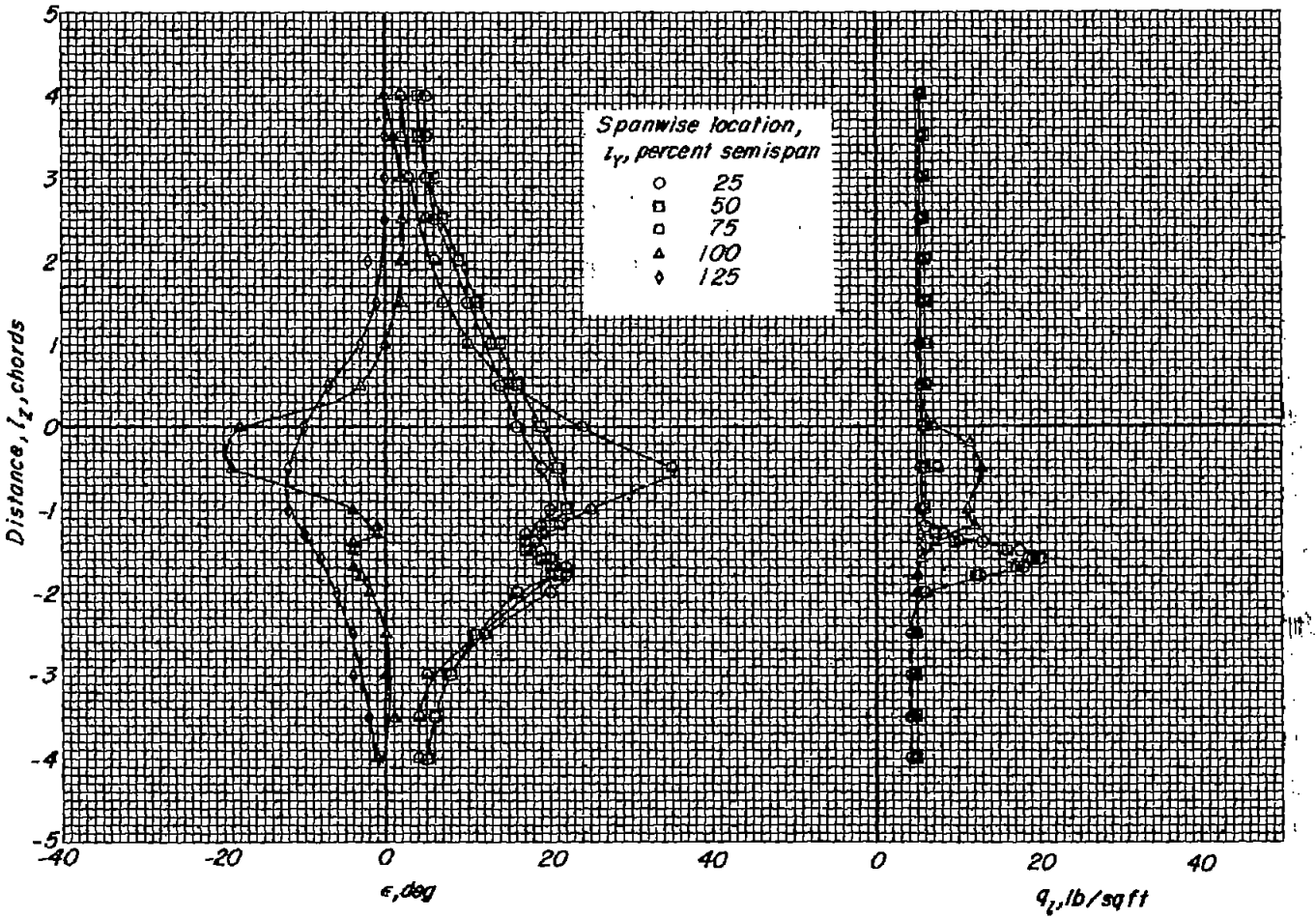


(a) $l_X$ = -3 chords.

Figure 14.- Variation of flow angle and local dynamic pressure with spanwise location at a momentum coefficient of 1.67. $\delta = 55^\circ$; $\alpha = 0^\circ$; q = 5 lb/sq ft.

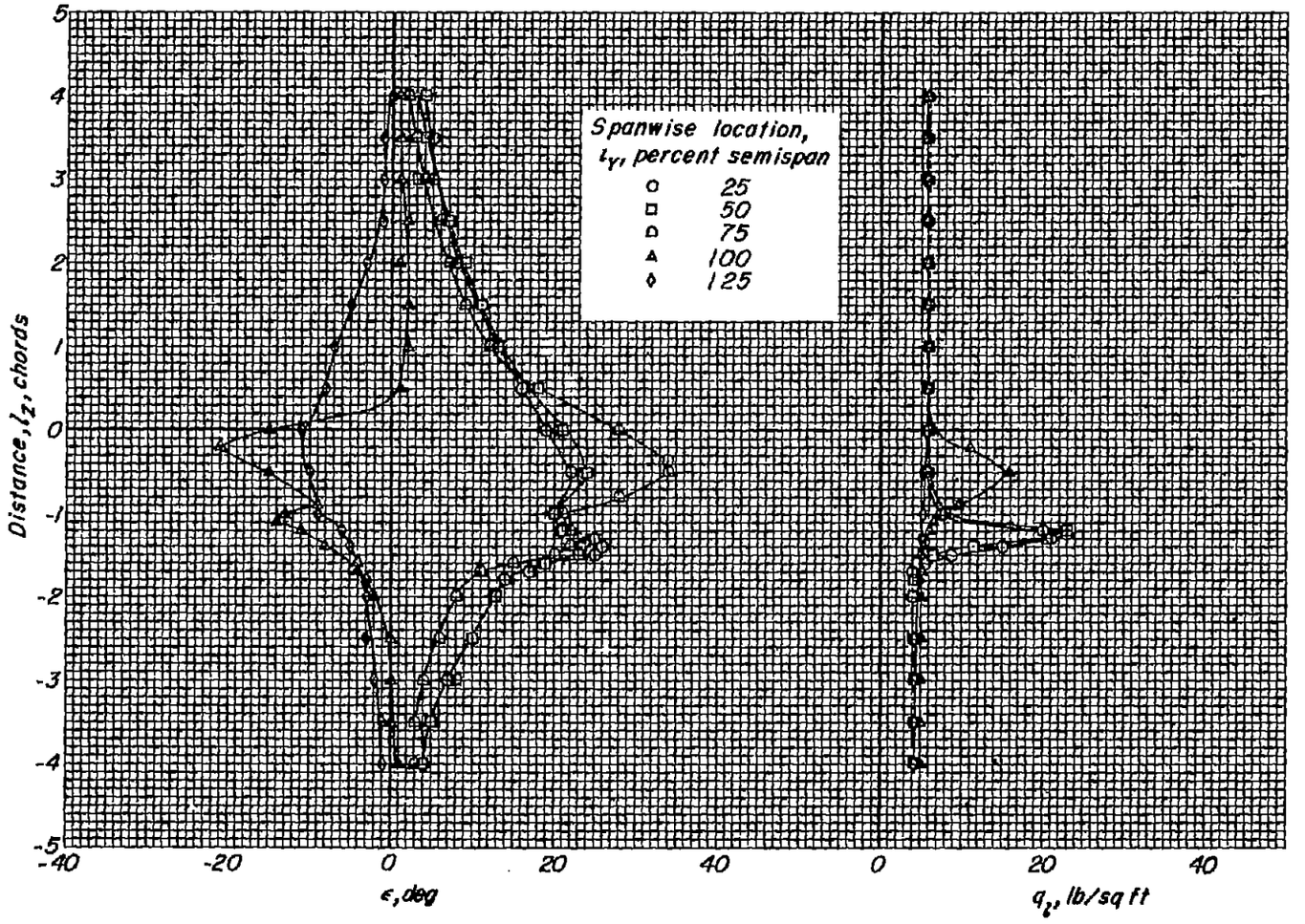


(b) $l_X$ = -2 chords.

Figure 14.- Continued.

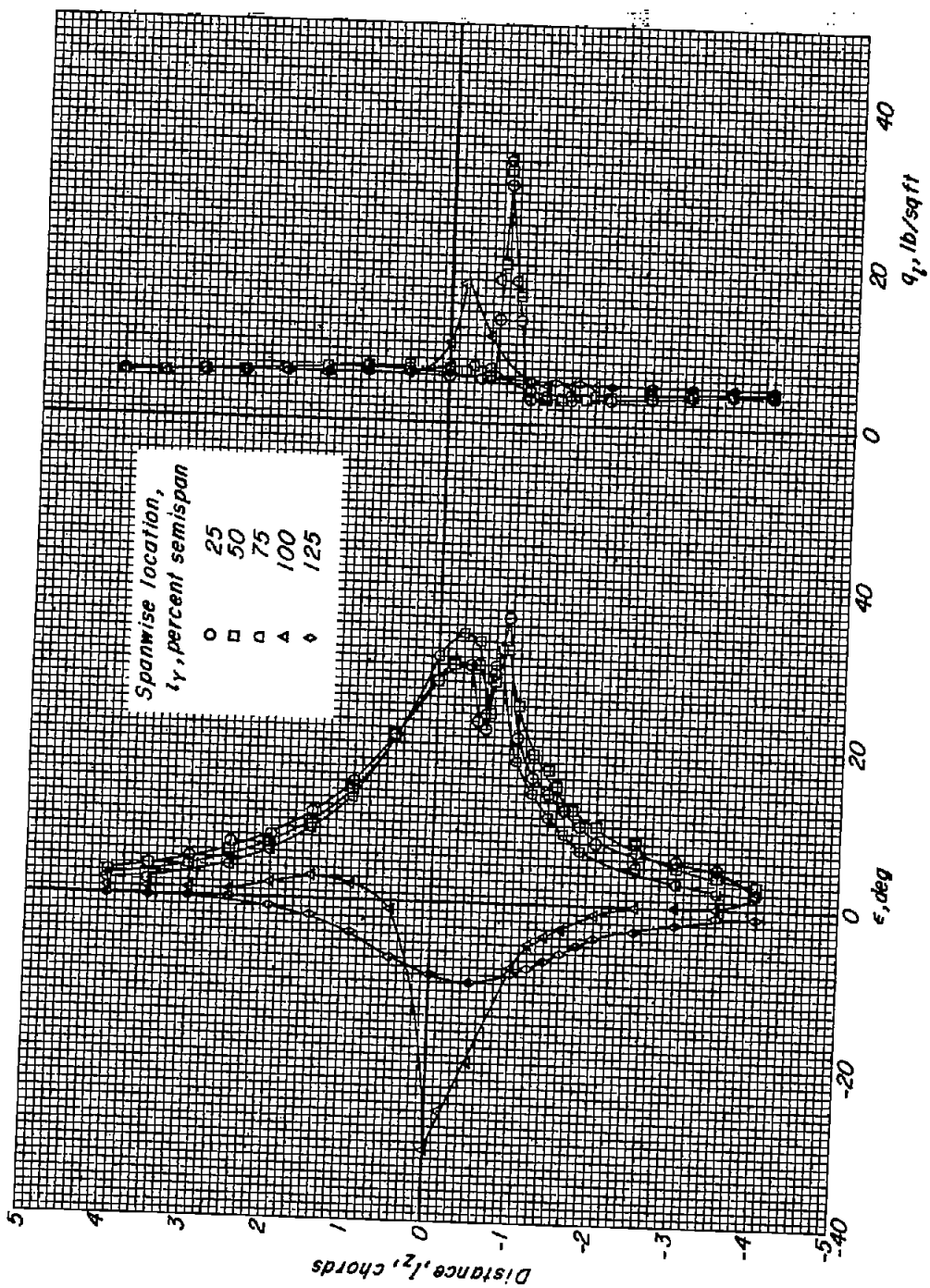


(c) $l_X$ = -1 chord.

Figure 14.- Concluded.

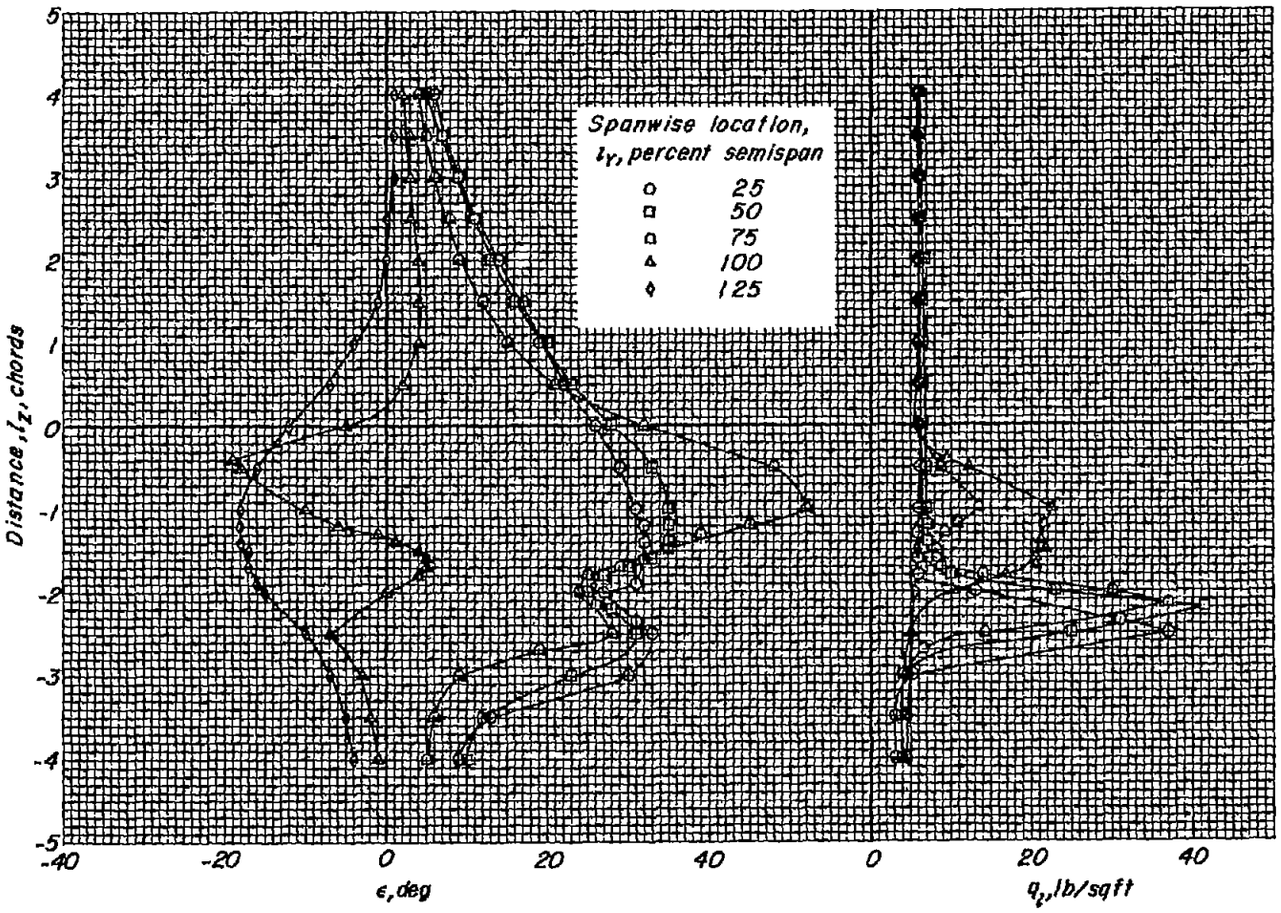


(a) $l_X = -3$ chords.

Figure 15.- Variation of flow angle and local dynamic pressure with spanwise location at a momentum coefficient of 6.46. $\delta = 55^\circ$; $\alpha = 0^\circ$; $q = 5$ lb/sq ft.

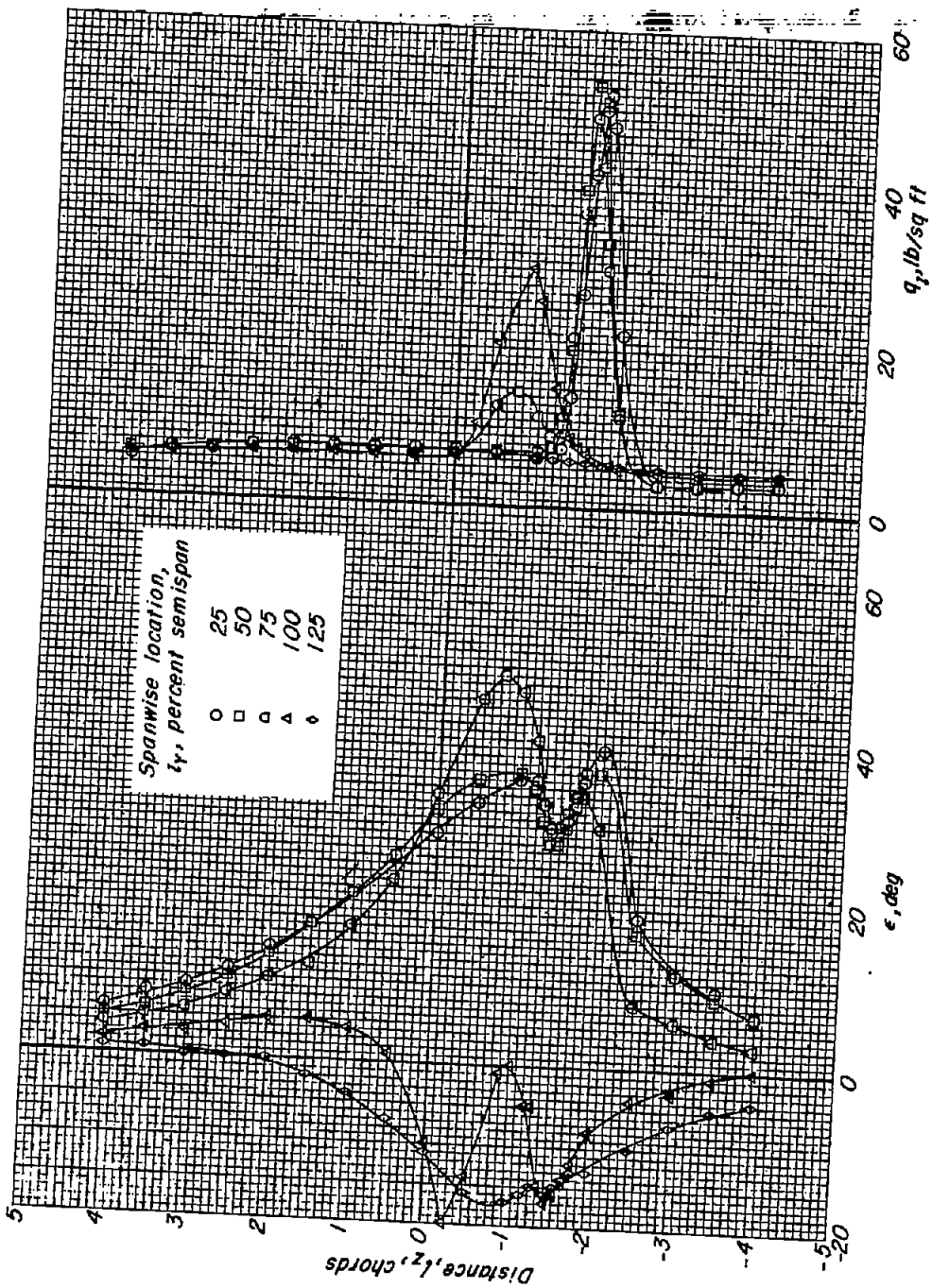


(b) $l_X$ = -2 chords.

Figure 15.- Continued.

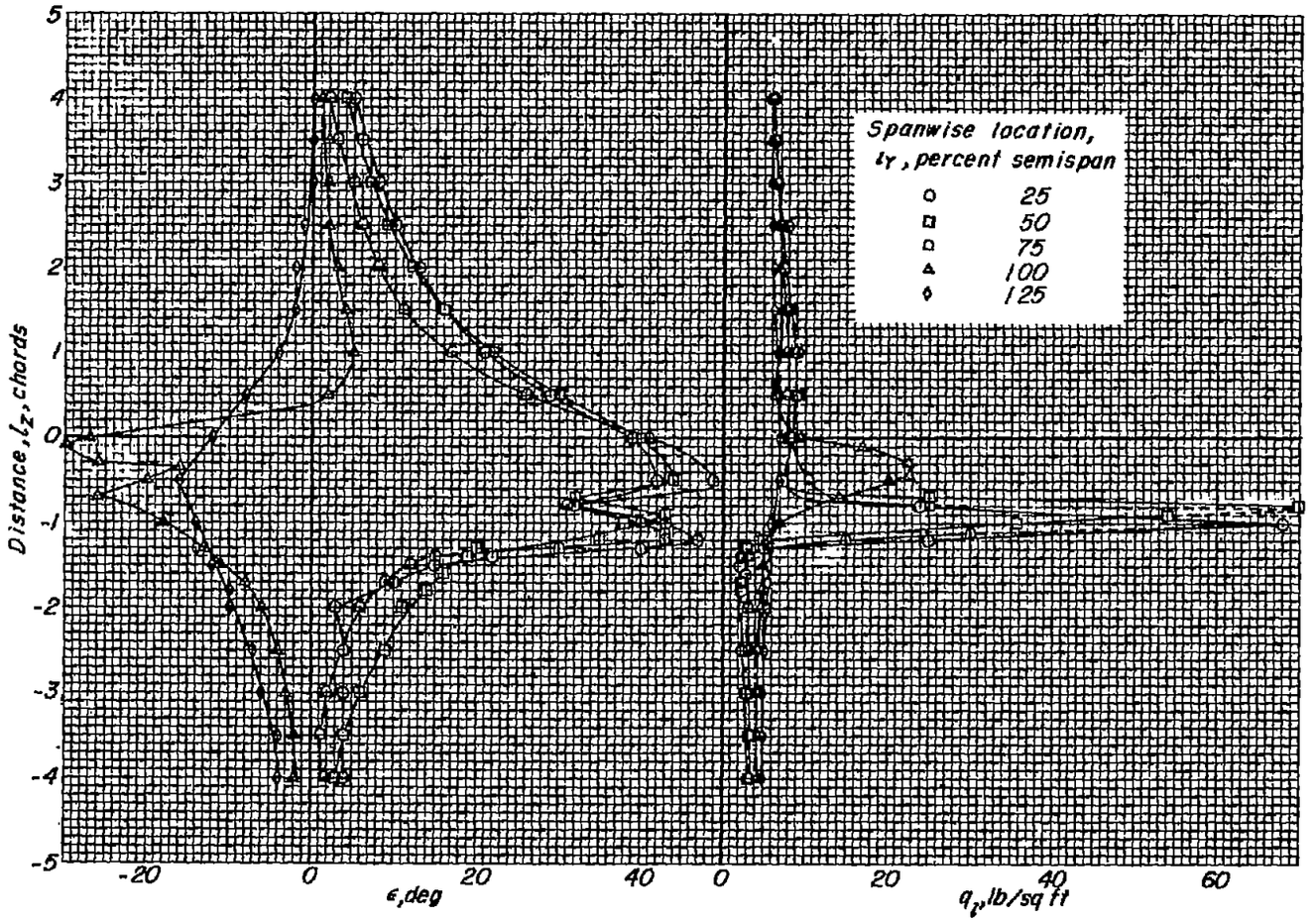


(c) $l_X$ = -1 chord.

Figure 15.- Concluded.

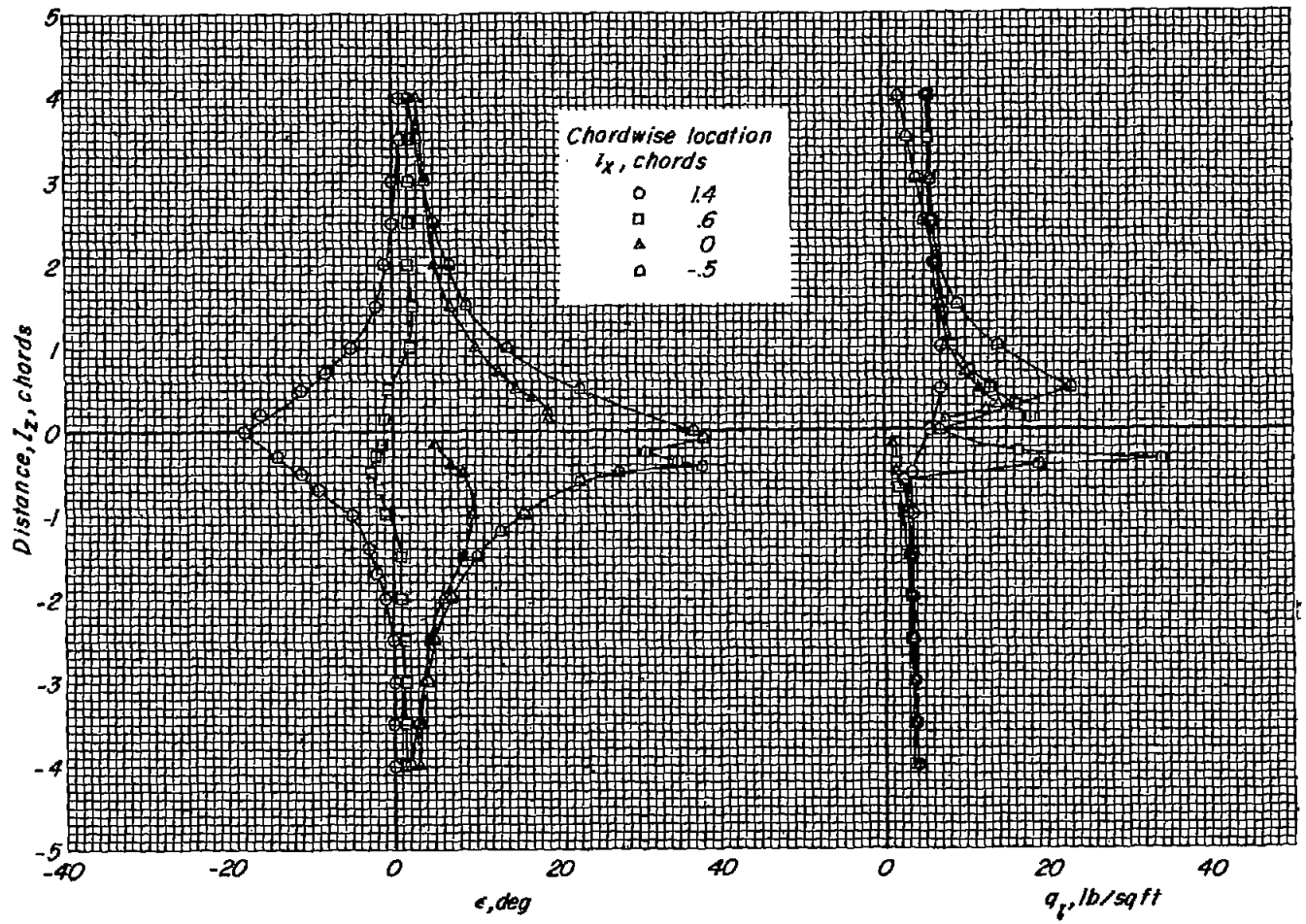


(a) $C_\mu = 1.67$.

Figure 16.- Variation of flow angle and local dynamic pressure with chordwise location on and near the wing. $\delta = 55^\circ$; $l_Y$ = 50-percent-semispan station; $\alpha = 0^\circ$; q = 5 lb/sq ft.

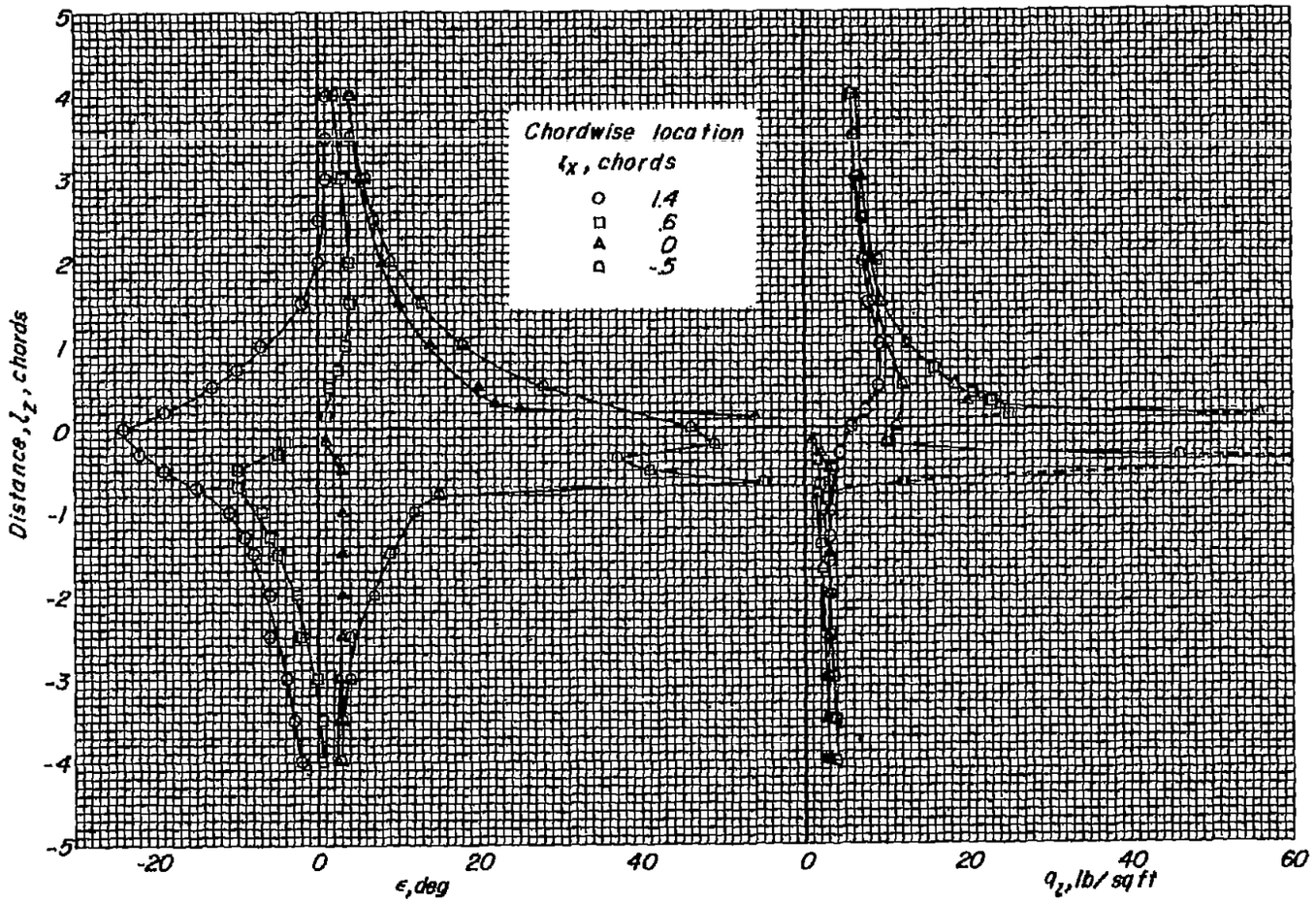


(b) $C_\mu = 6.46$.

Figure 16.- Concluded.

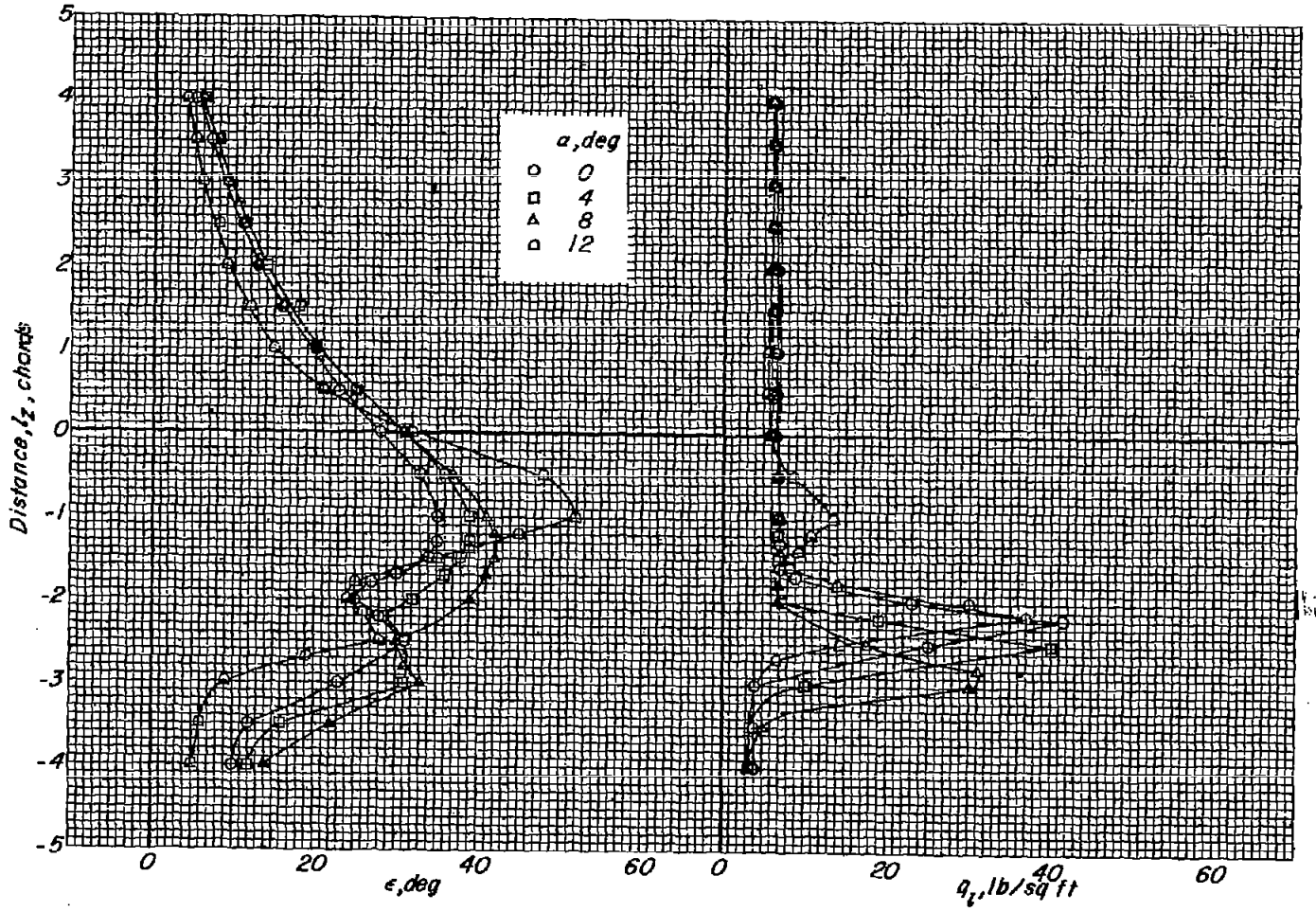


(a) $l_X$ = -3 chords.

Figure 17.- Effect of angle of attack on flow angle and local dynamic pressure at a momentum coefficient of 6.46. $\delta = 55^\circ$; $l_Y$ = 50-percent-semispan station; q = 5 lb/sq ft.

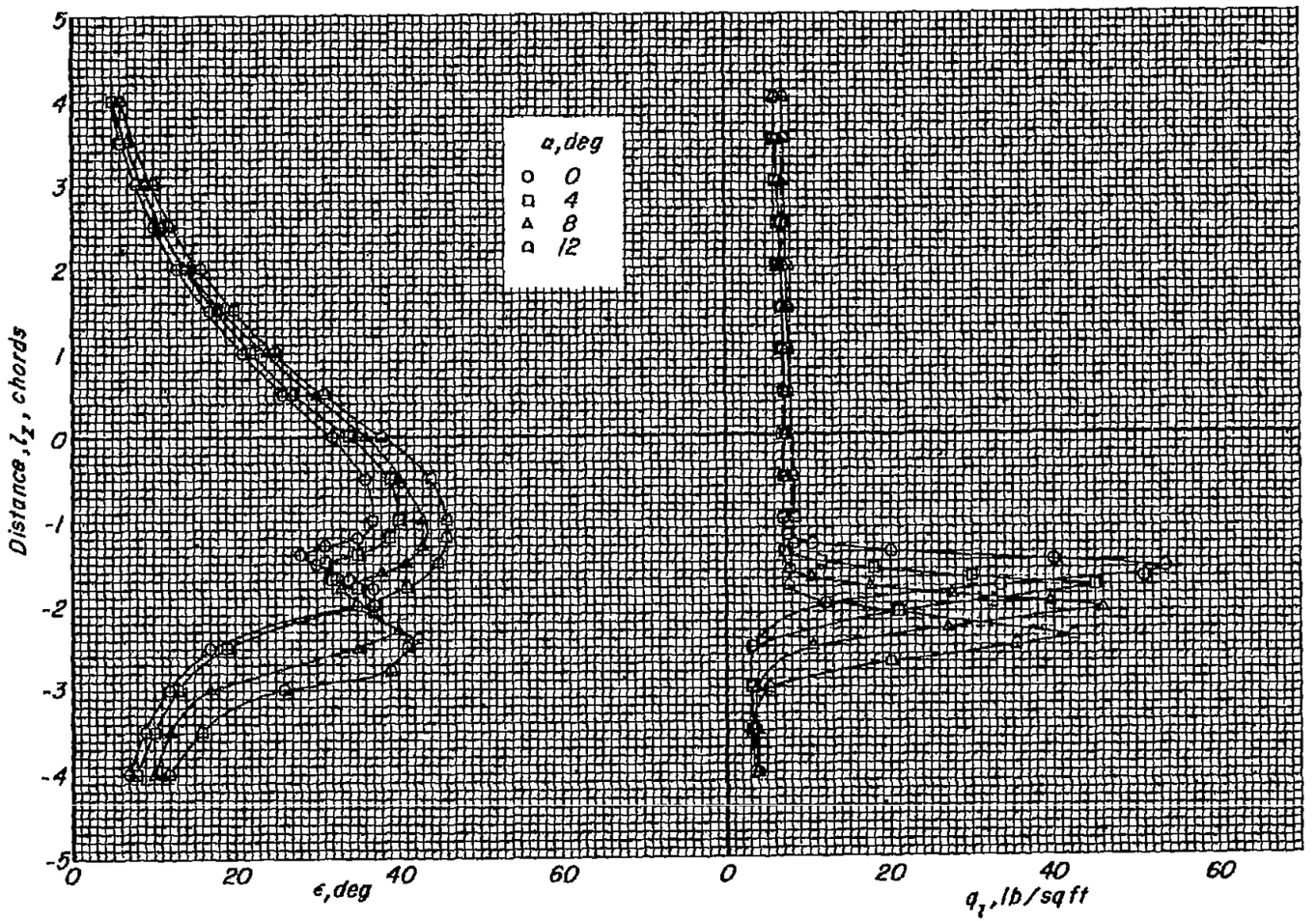


(b) $l_X$ = -2 chords.

Figure 17.- Concluded.

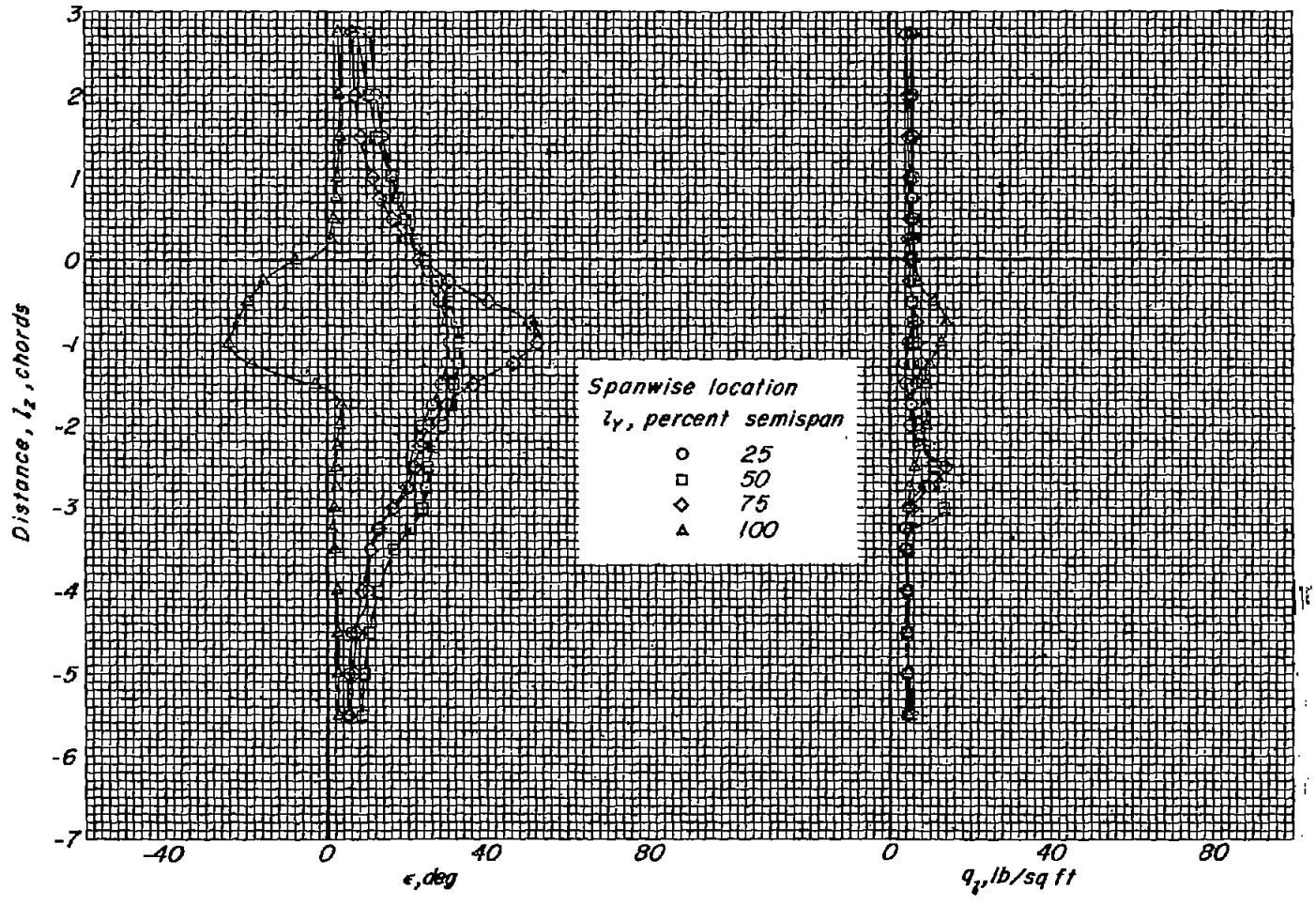


(a) $l_X$ = -3 chords.

Figure 18.- Variation of flow angle and local dynamic pressure with spanwise location at a momentum coefficient of 1.69. $\delta = 85^\circ$; $\alpha = 0^\circ$; q = 5 lb/sq ft.

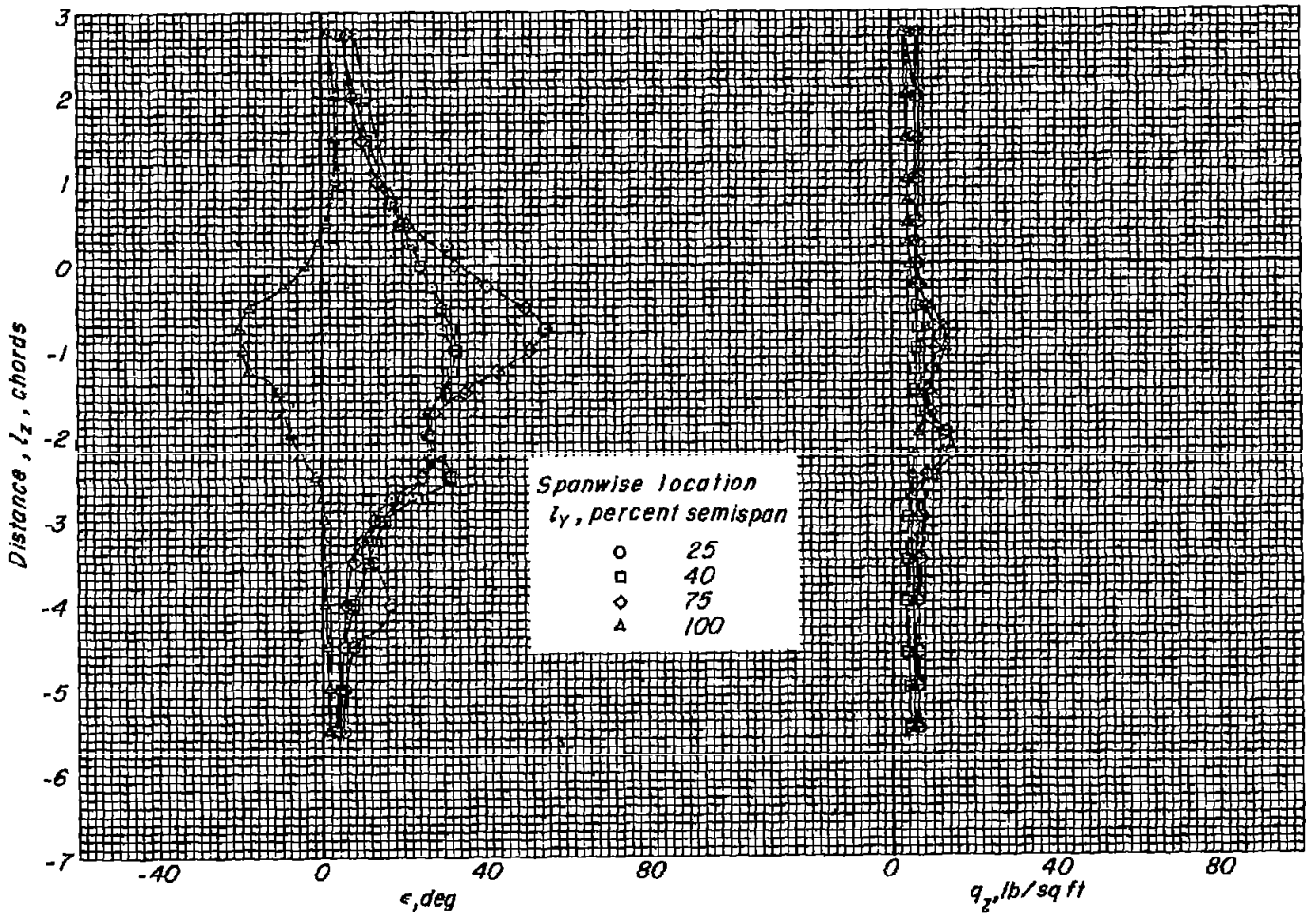


(b) $l_X$ = -2 chords.

Figure 18.- Continued.

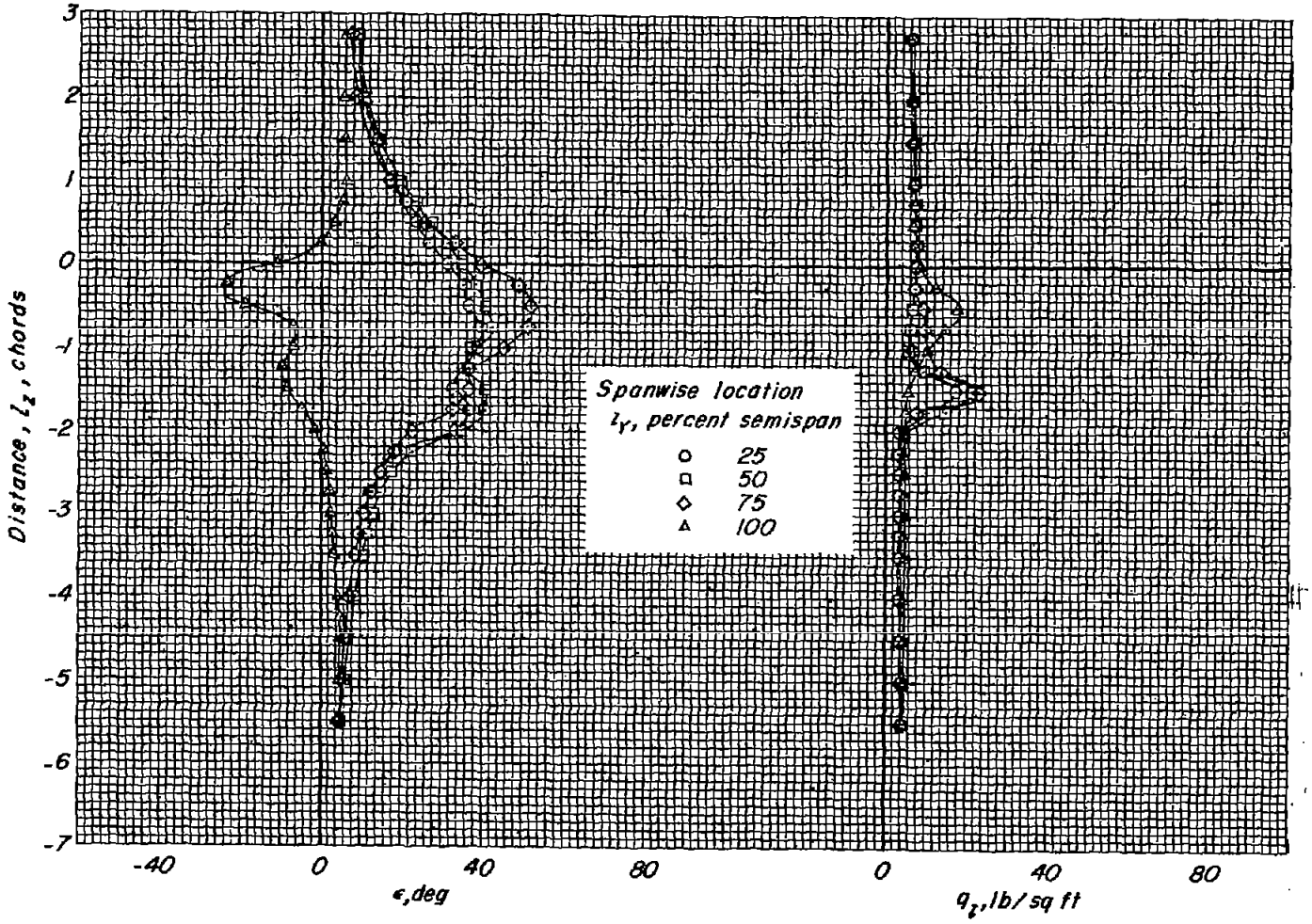


(c) $l_X$ = -1 chord.

Figure 18.- Concluded.

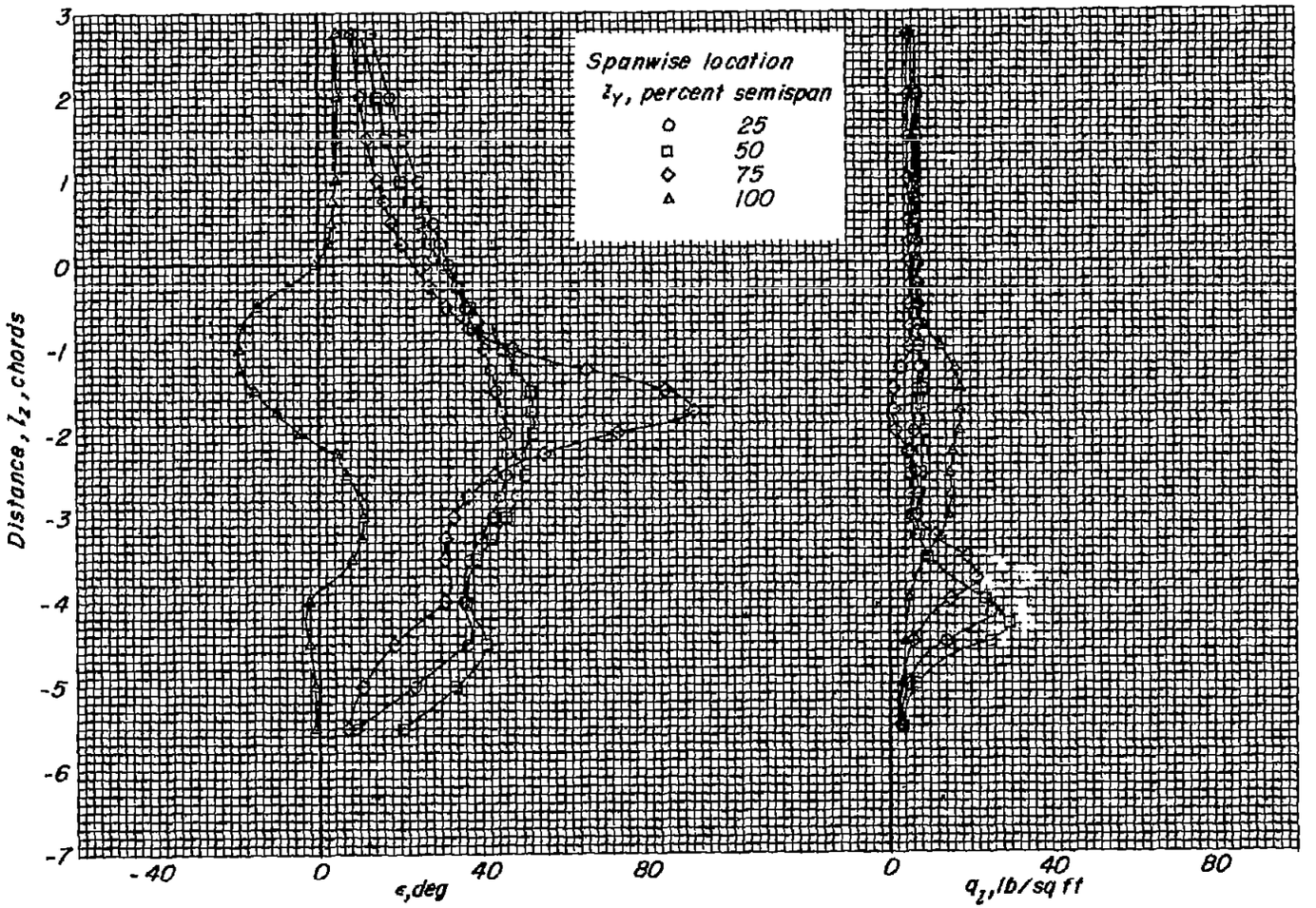


(a) $l_X$ = -3 chords.

Figure 19.- Variation of flow angle and local dynamic pressure with spanwise location at a momentum coefficient of 6.46. $\delta = 85^\circ$; $\alpha = 0^\circ$; q = 5 lb/sq ft.

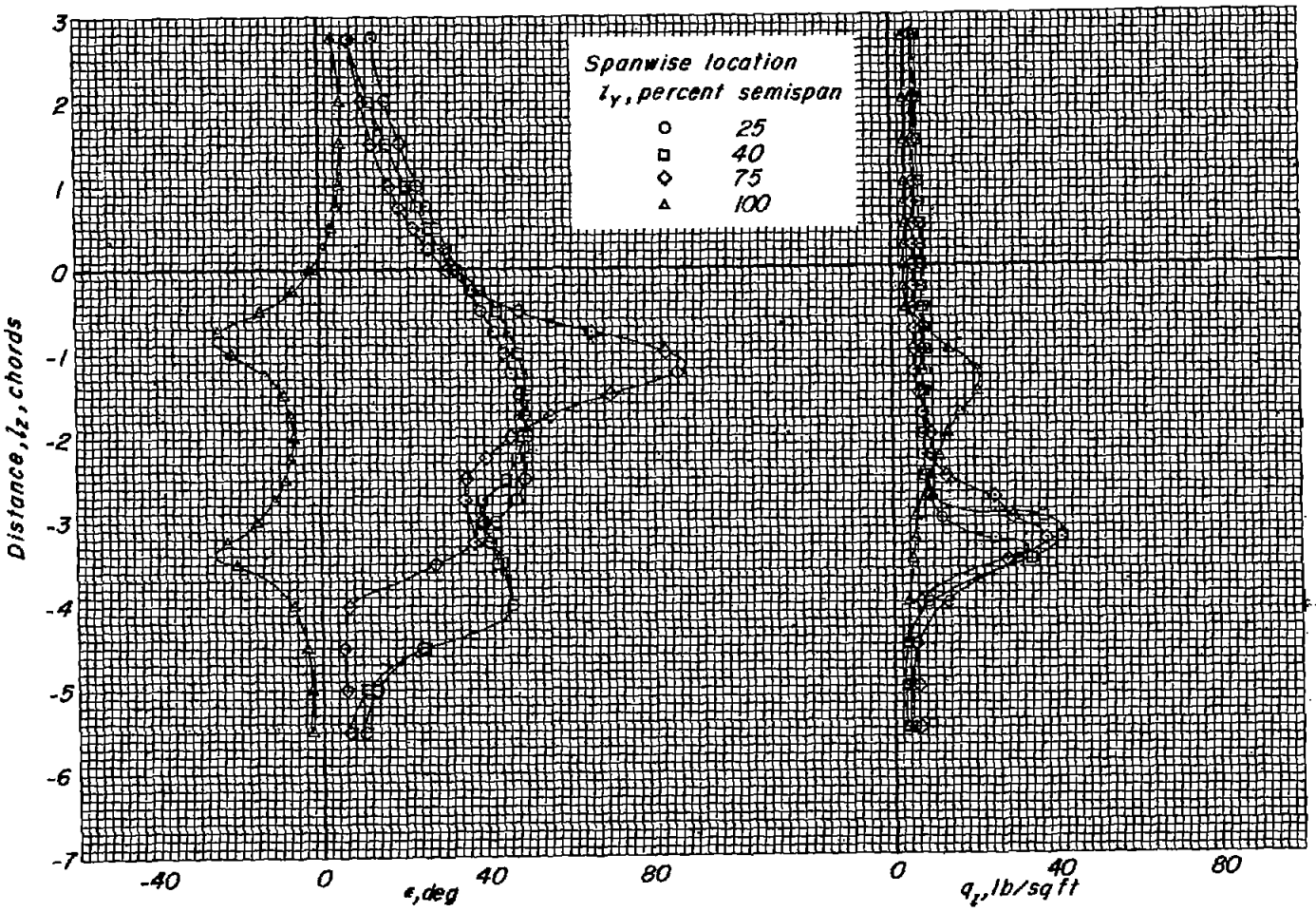


(b) $l_X$ = -2 chords.

Figure 19.- Continued.

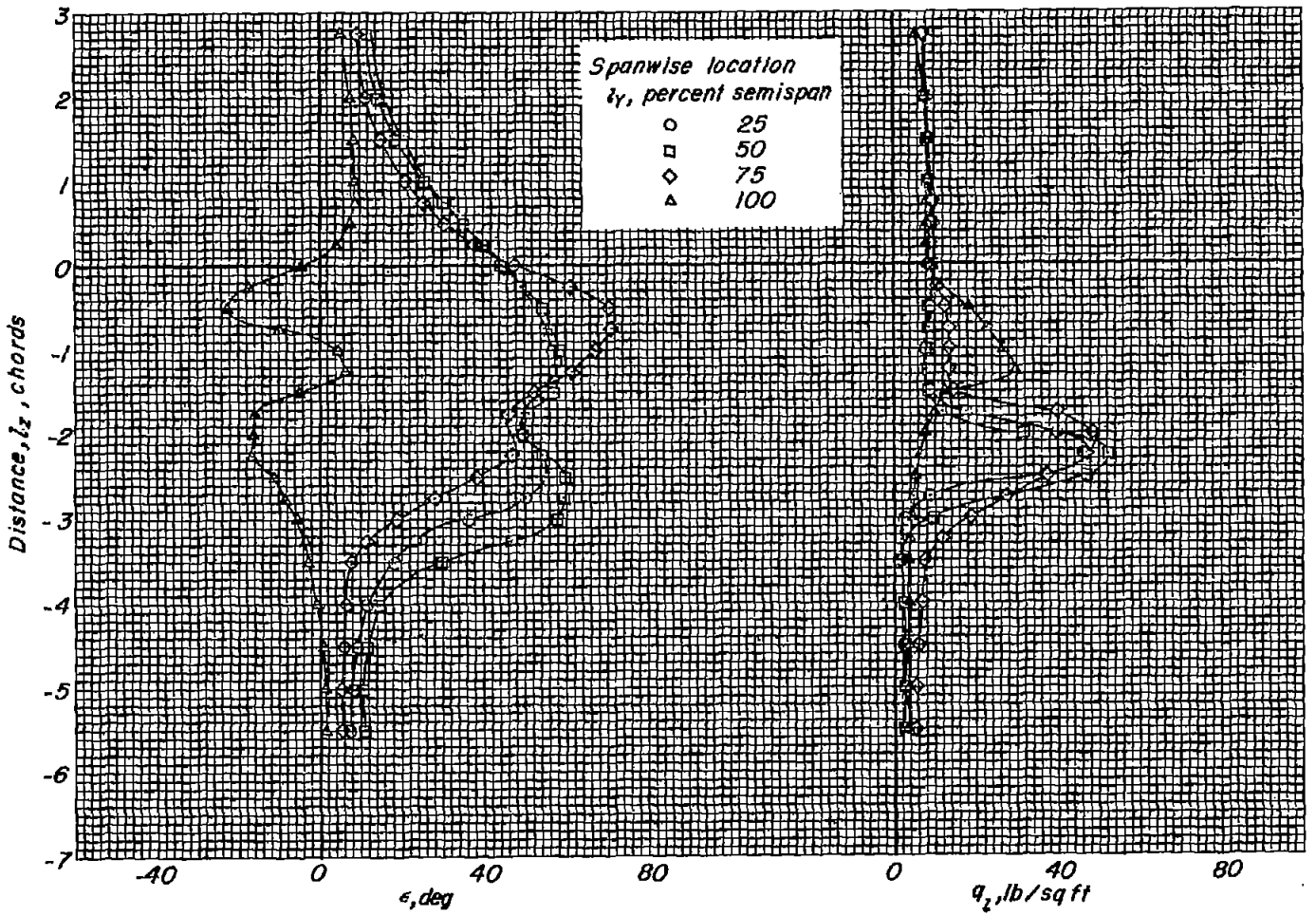


(c) $l_X$ = -1 chord.

Figure 19.- Concluded.

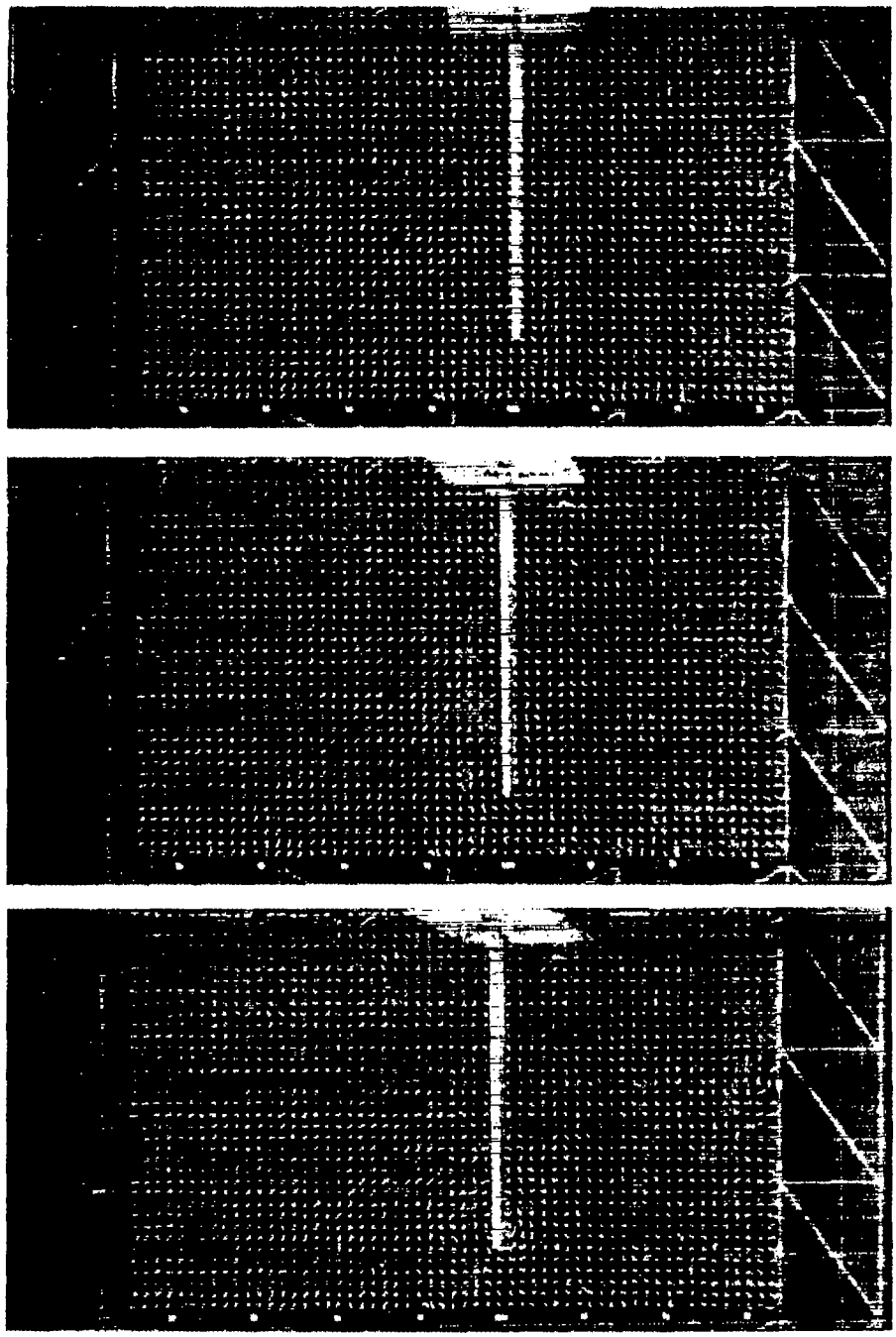


L-57-2718

Figure 20.- Photographs of tuft grid mounted 2.5 chords behind trailing edge of 7.25-inch-chord wing. $C_\mu = 0$; $q = 2$ lb/sq ft.

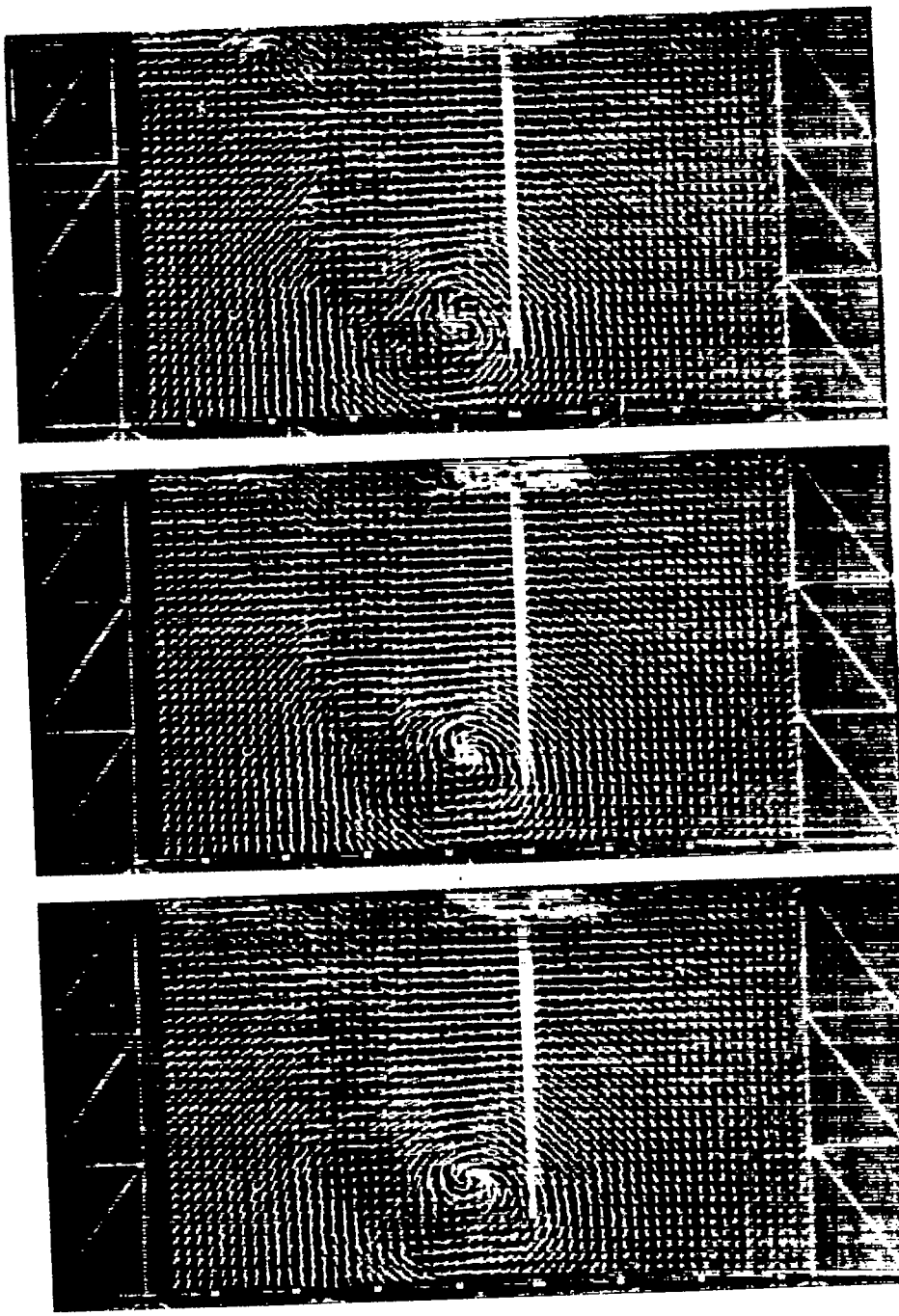


L-57-2719

Figure 21.- Photographs of tuft grid mounted 2.5 chords behind trailing edge of 7.25-inch-chord wing with jet-augmented flap deflected 55°. $C_\mu$ = 3.28; q = 2 lb/sq ft.

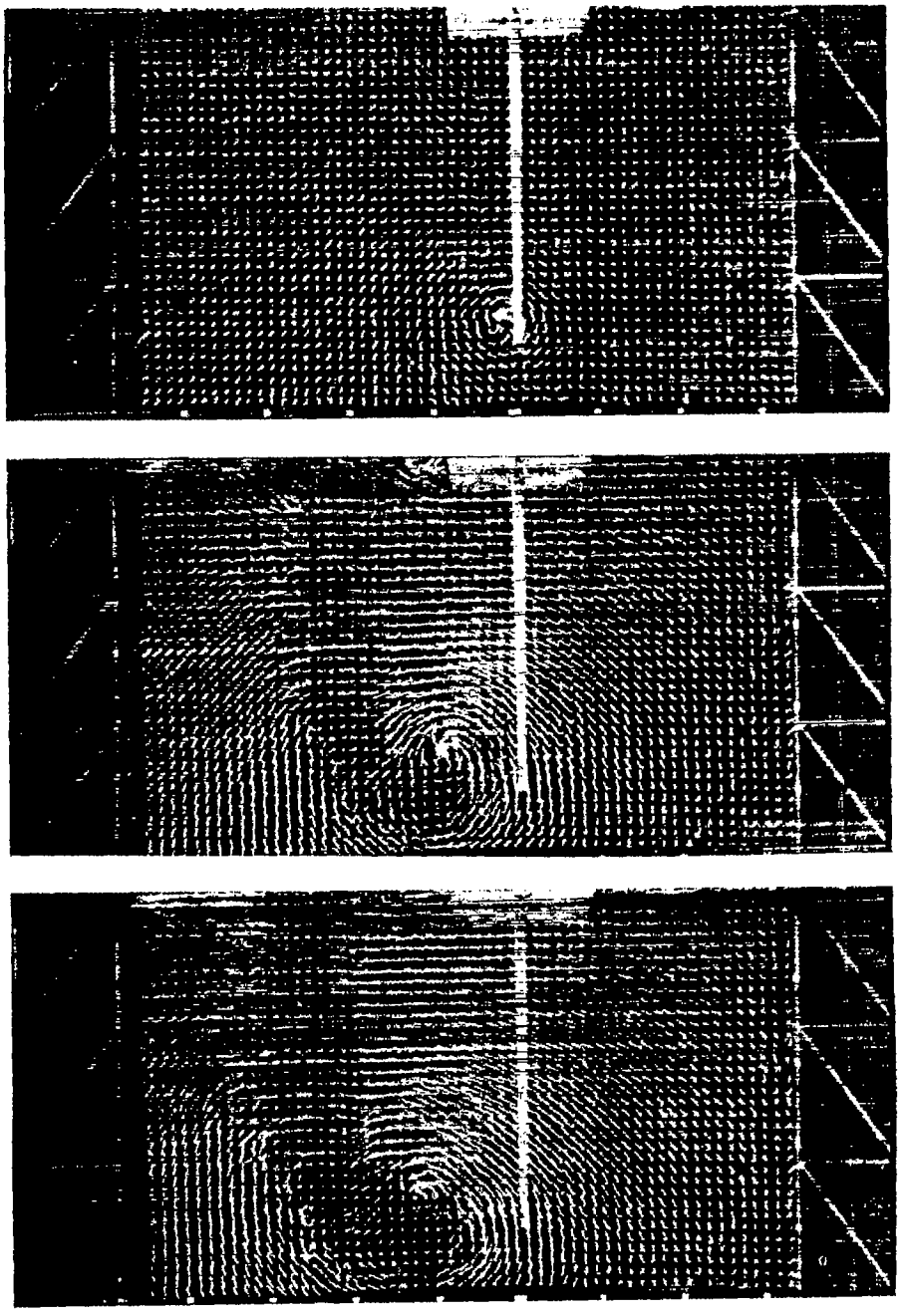


L-57-2720

Figure 22.- Photographs of tuft grid mounted 2.5 chords behind trailing edge of 7.25-inch-chord wing with jet-augmented flap deflected 55°. $\alpha = 0°$; q = 2 lb/sq ft.